Holographic reconstruction of black hole spacetime: machine learning and entanglement entropy

Byoungjoon Ahn,^a Hyun-Sik Jeong,^{b,c} Keun-Young Kim^{a,d} and Kwan Yun^a

E-mail: bjahn123@gist.ac.kr, hyunsik.jeong@csic.es, fortoe@gist.ac.kr, ludibriphy70@gm.gist.ac.kr

ABSTRACT: We investigate the bulk reconstruction of AdS black hole spacetime emergent from quantum entanglement within a machine learning framework. Utilizing neural ordinary differential equations alongside Monte-Carlo integration, we develop a method tailored for continuous training functions to extract the general isotropic bulk metric from entanglement entropy data. To validate our approach, we first apply our machine learning algorithm to holographic entanglement entropy data derived from the Gubser-Rocha and superconductor models, which serve as representative models of strongly coupled matters in holography. Our algorithm successfully extracts the corresponding bulk metrics from these data. Additionally, we extend our methodology to many-body systems by employing entanglement entropy data from a fermionic tight-binding chain at half filling, exemplifying critical one-dimensional systems, and derive the associated bulk metric. We find that the metrics for a tight-binding chain and the Gubser-Rocha model are similar. We speculate this similarity is due to the metallic property of these models.

^aDepartment of Physics and Photon Science, Gwangju Institute of Science and Technology, 123 Cheomdan-gwagiro, Gwangju 61005, Korea

^bInstituto de Física Teórica UAM/CSIC, Calle Nicolás Cabrera 13-15, 28049 Madrid, Spain

^cDepartamento de Física Teórica, Universidad Autónoma de Madrid, 28049 Madrid, Spain

^dResearch Center for Photon Science Technology, Gwangju Institute of Science and Technology, 123 Cheomdan-gwagiro, Gwangju 61005, Korea

Co	onte	\mathbf{nts}						
1	Introduction							
2	Holographic entanglement entropy: a quick review							
3	Bilson's method							
	3.1 Preliminary for the Bilson's method							
	3.2 Reconstruction formula							
	3.3	3.3 Example: Linear-axion model						
4	Machine learning method							
	4.1 Methodology: Neural ODEs and Monte-Carlo integration							
	4.2	Emergent spacetime from holographic entanglement entropy						
		4.2.1	Linear-axion model	16				
		4.2.2	Gubser-Rocha model	17				
		4.2.3	Holographic superconductors	19				
	4.3	Emerg	Emergent spacetime from a one-dimensional chain					
		4.3.1	Machine learning setup	22				
		4.3.2	Emergent metric from a fermionic tight-binding chain at half filling	24				
5	Conclusions							
\mathbf{A}	Entanglement entropy in the small subsystem size limit							
В	3 The procedure of training the network and the error estimation 29							

1 Introduction

Entanglement, a fundamental characteristic of quantum mechanics, elucidates the intriguing non-local correlations between quantum entities, and is at the core of quantum information sciences [1–3]. Especially, the notion of *entanglement entropy* now exerts a wide-ranging influence, spanning from condensed matter [4] to high-energy quantum field theory [5] and even extending into quantum gravity [6].

Within condensed matter physics, for example, entanglement entropy proves its versatility as a tool, facilitating the characterization of quantum phases and the intricate dynamics of strongly correlated many-body systems [7, 8]. The scaling behavior of entanglement entropy [9] offers insights into phases beyond symmetry characterization, particularly useful for identifying exotic states like topological phases [10–12] and spin liquids [13, 14]. Additionally, entanglement entropy aids in exploring quantum criticality [15], understanding non-equilibrium dynamics [16, 17], and assessing numerical techniques for efficient many-body physics simulation [18].

Holographic entanglement entropy. Nevertheless, the concept of entanglement entropy has also garnered increased attention in recent decades due to its significant role in holography (AdS/CFT correspondence) [19–21]. Holography entails a duality between boundary quantum field theories and bulk gravitational theories, offering a compelling framework for understanding the emergence of spacetime geometry from quantum entanglement. Particularly notable is its connection exemplified in the Ryu-Takayanagi (RT) formula [22], which establishes a relationship between the entanglement entropy of a subsystem in the boundary field theory and the area of the minimal surface in the bulk corresponding to the same region.¹

By leveraging the RT formula and understanding gravity through the lens of quantum entanglement, the holographic examination of entanglement entropy not only offers a more manageable approach to studying and computing this measure, but also yields general lessons applicable other branches of physics such, as quantum field theories and strongly coupled many-body physics [31]. For instance, the c-theorem, established in two-dimensional conformal field theory, is derived from analyzing how entanglement entropy evolves under renormalization group flows [32]. Also, holographic entanglement entropy proves instrumental in the study of the aforementioned condensed matter physics by characterizing various phases of matter, exemplified by holographic superconductors [33].² This elucidates phenomena such as phase transitions, quantum criticality, and topological order, offering valuable insights into the entanglement properties of strongly correlated quantum systems.

Bulk reconstruction in holography. It is worth noting that, in most studies of holographic entanglement entropy, the standard approach is the bottom-up methodology. In this framework, gravitational bulk theories are employed to depict the realistic dual boundary quantum systems (e.g., characterized by broken translational symmetries), and the RT formula is used to study the associated entanglement entropy.

Nonetheless, despite significant advancements over the past decade, which provide compelling evidence that the entanglement structure of the underlying quantum mechanical degrees of freedom plays a pivotal role in shaping the emergent holographic spacetime geometry and its dynamics, an open question remains. Specifically, it is still unclear which bulk gravity model can accurately reproduces the entanglement features of a given quantum system on the boundary and how to identify such models.

One essential approach for identifying such bulk gravity theories is termed 'bulk reconstruction', representing a non-trivial inverse problem entailing holographic mapping from lower (boundary) to higher (bulk) dimensions. A captivating aspect within this endeavor is the reconstruction of the metric in the holographic spacetime.³ There are numerous

¹The RT formula, along with its subsequent generalizations [23–26], provides a deeper elucidation of the pivotal role of entanglement in holographic duality. Another noteworthy entanglement measure is the reflected entropy, which possesses a gravity dual known as the entanglement wedge cross section [27–30].

²Please refer to [34] for a comprehensive list of additional references regarding the investigation of entanglement in diverse holographic matters.

³Additional significant branches can be found in [35–38], with particular emphasis on bulk operator reconstruction.

methodologies for bulk metric reconstruction, leveraging diverse boundary physical quantities. These include the source and expectation value of the energy-momentum tensor [39], singularities in sets of correlation functions [40, 41], entanglement entropy of boundary intervals [42–45], differential entropy, a UV-finite combination of entanglement entropy [47–49], divergence structure of boundary n-point functions [50, 51], modular Hamiltonians of boundary subregions [52, 53], Wilson loops related to quark potential [54], four-point correlators in an excited quantum state [55], and holographic complexities [56, 57], among others. It is noteworthy that much of the research on metric reconstruction has been motivated by the notion that spacetime is constructed from quantum entanglement [22, 58–62].

Machine learning and holography. In recent years, machine learning has emerged as a promising approach to addressing bulk reconstruction by identifying the underlying bulk theory, such as reconstructing the bulk metric. Efficient holographic modeling has been successfully demonstrated through the application of machine learning techniques with various physical quantities, including lattice QCD data of the chiral condensate, hadron spectra, meson spectrum, shear viscosity, optical conductivity, and entanglement entropy, and so forth [66–85].⁶

Machine learning holography not only facilitates the construction of data-driven holographic models but also provides insights into deeper understanding of holography itself. This approach is referred to as the AdS/DL correspondence, and establishes connections between deep learning (DL) – a form of machine learning utilizing deep neural networks – and holography. Here, deep learning functions as a solver for the inverse problem, enabling the determination of the bulk metric upon training the neural network. Readers interested in grasping the essential concept of AdS/DL within a simplified framework are encouraged to refer [90], which illustrates this concept through a classical mechanics problem.

Motivation of this paper. In this manuscript, we investigate the reconstruction of the holographic bulk metric through machine learning of the boundary entanglement entropy. Our aim is to assess the effectiveness of machine learning in this context.

Note that a machine learning method has been applied in related contexts [77, 78], where authors inferred the dual geometry from a given entanglement entropy using the RT formula and deep learning methods. However, due to inherent discontinuities in their algorithm, the reconstructed metric lacks continuity. Additionally, for simplicity, the entanglement entropy was assumed to have the dual geometry when only the blackening factor f(z) is unknown, for instance, h(z) = 1 in (2.1). We intend to enhance this work by incorporating a neural ODE approach and a more generic metric setup, i.e., any func-

⁴See also the recent work [46] where the holographic metric is constructed from the derivative of entanglement entropy in lattice Yang-Mills theory.

⁵Another notable progression in investigating bulk reconstruction in holography involves a novel approach from quantum many-body systems, termed the multi-scale entanglement renormalization ansatz (MERA) of tensor networks [60, 63–65].

⁶Other related works that extract the spacetime metric using machine learning, independent of holography, can be found in [86–89].

tion of f(z) and h(z), making it more compatible with bulk reconstruction programs for continuous and generic metrics.

It is also worth mentioning that when h(z) = 1, one may not need to resort to machine learning holography; instead, Bilson's method [44] can be utilized to invert the RT formula, generating the metric as output and entanglement entropy as input. Nevertheless, for completeness, we review Bilson's method in the main text and discuss its limitations when $h(z) \neq 1$, motivating the use of machine learning holography to find the complete metric from entanglement entropy.

As illustrative examples for our purpose, in this study, we initially employ two representative holographic entanglement entropy models with $h(z) \neq 1$: the Gubser-Rocha model [92] and the holographic superconductor model [93, 94], where the former has been particularly instrumental in examining the characteristics of strange metals.⁸ Moreover, in addition to the aforementioned holographic matter models, we incorporate entanglement entropy data from quantum many-body systems. Specifically, we utilize data obtained from a fermionic tight-binding chain at half filling in critical one-dimensional systems [98] to ascertain the corresponding emergent bulk metric.

In essence, we propose applying data-driven and machine learning methodologies to unveil the emergent continuous metric based on boundary entanglement entropy data. Analyzing various entanglement entropy dataset within the *generic and continuous* metric configuration, our objective is to establish machine learning holography as both a practical and theoretical framework. Through our investigation, we aim to offer valuable insights into the fundamental aspects of quantum entanglement, thereby deepening our understanding of many-body quantum physics and potentially advancing the exploration of holographic duality.

This paper is organized as follows. Section 2 presents a quick review of the RT formula concerning the holographic entanglement entropy. Additionally, in section 3, we discuss Bilson's method for generating the metric from entanglement entropy and address its limitation in studying the complete metric. Section 4 introduces a machine learning method tailored to determine the continuous/generic metric based on provided entanglement entropy. As input data of machine learning method, we utilize both the holographic entanglement entropy and entanglement entropy from a fermionic tight-binding chain. Finally, Section 5 is devoted to conclusions.

⁷In the scenario of isotropic geometries, (2.1) represents the most general metric setup. Specifically, metrics where $(g_{tt} \neq g_{zz} \neq g_{xx})$ can always be expressed in the form of (2.1) through coordinate transformations. For detailed discussions, refer to [91].

 $^{^8}$ It is noteworthy that the Gubser-Rocha model [92] can be derived through a top-down approach. Specifically, for d=3, it results from a consistent truncation of eleven-dimensional supergravity compactified on $AdS_4 \times S^7$ [92], while for d=4, it is derived from ten-dimensional type IIB String Theory as the near-horizon limit of D3-branes [92, 95]. See also [96, 97] for discussions on top-down holographic superconductors from string/M-theory. Consequently, our study can also be regarded as an exploration of such top-down models through the lens of machine learning.

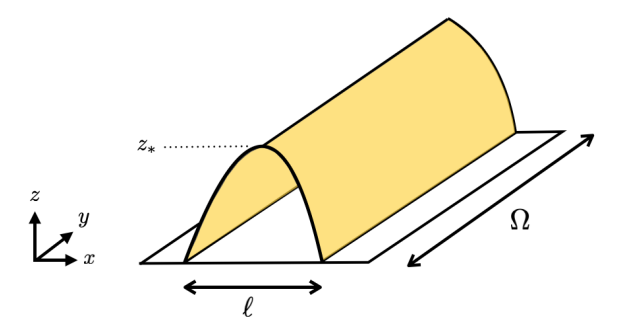


Figure 1. A strip-shaped entangling region with its minimal surface depicted in yellow. The strip has a width ℓ in the x-direction and Ω in another direction. z_* represents the maximum z value attained by the minimal surface.

2 Holographic entanglement entropy: a quick review

We consider the asymptotically AdS_4 spacetime as

$$ds^{2} = \frac{L^{2}}{z^{2}} \left[-f(z) dt^{2} + \frac{dz^{2}}{f(z)} + h(z) \left(dx^{2} + dy^{2} \right) \right], \qquad (2.1)$$

where L represents the AdS radius and the functions f(z) and h(z) are expanded as f = h = 1 near the AdS boundary $(z \to 0)$.

For the later use, within the metric (2.1) we also read the thermodynamic quantities as the temperature (T) and the thermal entropy (s) as

$$T = -\frac{f'(z)}{4\pi} \bigg|_{z_h}, \qquad s = \frac{L^2}{4G_N} \frac{h(z)}{z^2} \bigg|_{z_h},$$
 (2.2)

which are evaluated at the event horizon z_h , where G_N is the Newton's constant.

Holographic entanglement entropy. The holographic dictionary to study the entanglement entropy (S) is the Ryu-Takayanagi formula [22, 62]. The formula allows us to compute the entanglement entropy of the entangling region on the boundary by examining the corresponding region the bulk spacetime as

$$S = \frac{\text{Area}(\gamma)}{4G_N} \,, \tag{2.3}$$

where γ is the area if the minimal surface in the bulk, which is anchored at the AdS boundary. In this paper, we focus on a strip-shape entangling region. See Fig. 1: the minimal surface takes the form of a yellow surface with a width ℓ in x-direction and extends infinitely Ω in y-directions. z_* represents the maximal z value of this minimal surface in the bulk.

Within the metric (2.1), it is straightforward [22, 62] to find the geometric quantities for (2.3), S and ℓ , as

$$S = \frac{L^2 \Omega}{2G_N} \int_{\epsilon}^{z_*} \frac{1}{z^2} \sqrt{\frac{h(z)}{1 - \frac{z^4}{z_*^4} \frac{h(z_*)^2}{h(z)^2}}} \frac{1}{\sqrt{f(z)}} dz, \qquad \ell = 2 \int_0^{z_*} \frac{1}{\sqrt{\frac{h(\alpha)^2}{h(z_*)^2} \frac{z_*^4}{\alpha^4} - 1}} \frac{1}{\sqrt{h(\alpha)f(\alpha)}} d\alpha, \tag{2.4}$$

where ϵ is the UV cutoff. In order to isolate the UV divergence, it is convenience to split the integrand of S in (2.4) into two parts as

$$S = \frac{L^{2}\Omega}{2G_{N}} \left[\int_{\epsilon}^{z_{*}} \frac{1}{z^{2}} dz + \int_{0}^{z_{*}} \frac{1}{z^{2}} \left(\sqrt{\frac{h(z)}{1 - \frac{z^{4}}{z_{*}^{4}} \frac{h(z_{*})^{2}}{h(z)^{2}}} \frac{1}{\sqrt{f(z)}} - 1 \right) dz \right]$$

$$= \frac{L^{2}\Omega}{2G_{N}} \left[\frac{1}{\epsilon} + \left\{ \int_{0}^{z_{*}} \frac{1}{z^{2}} \left(\sqrt{\frac{h(z)}{1 - \frac{z^{4}}{z_{*}^{4}} \frac{h(z_{*})^{2}}{h(z)^{2}}} \frac{1}{\sqrt{f(z)}} - 1 \right) dz - \frac{1}{z_{*}} \right\} \right]$$

$$:= \frac{L^{2}\Omega}{2G_{N}} \left[\frac{1}{\epsilon} + S_{\text{Finite}} \right],$$

$$(2.5)$$

where the UV divergence reads as $1/\epsilon$.

3 Bilson's method

It is instructive to note that the Ryu-Takayanagi formula (2.4) establishes a relationship where the entanglement entropy is derived from a given metric. In other words, the metric serves as the input data, while the entanglement entropy emerges as the output.

3.1 Preliminary for the Bilson's method

On the other hands, Bilson's method [44] attempts to invert the Ryu-Takayanagi formula (2.4), flipping the roles of metric and entanglement entropy. Here, the metric becomes the output, while the entanglement entropy becomes the input.

Bilson's method involves two main ingredients. Firstly, it employs the handbook of integral equations [99] to express:

$$F(z_*) = \int_{\epsilon}^{z_*} \frac{1}{\sqrt{G(z_*) - G(z)}} Y(z) \, dz, \qquad G'(z_*) > 0$$
(Solution):
$$Y(z_*) = \frac{1}{\pi} \frac{d}{dz_*} \int_{\epsilon}^{z_*} \frac{G'(z)}{\sqrt{G(z_*) - G(z)}} F(z) \, dz.$$
(3.1)

Another key aspect involves

$$\frac{\mathrm{d}S}{\mathrm{d}\ell} = \frac{\mathrm{d}z_*}{\mathrm{d}\ell} \frac{\mathrm{d}S}{\mathrm{d}z_*} = \frac{L^2 \Omega}{4G_N} \frac{h(z_*)}{z_*^2},\tag{3.2}$$

where we used the chain rule with

$$\frac{\mathrm{d}S}{\mathrm{d}z_{*}} = \frac{L^{2}\Omega}{2G_{N}} \sqrt{h(z_{*})} \left[\lim_{z \to z_{*}} \frac{1}{\sqrt{z_{*}^{4} - z^{4} \frac{h(z_{*})^{2}}{h(z)^{2}}}} \frac{1}{\sqrt{f(z_{*})}} + z_{*}^{4} h(z_{*})^{2} \int_{0}^{z_{*}} \sqrt{\frac{4z^{10} h(z)^{6} (2h(z_{*}) - z_{*} h'(z_{*}))^{2}}{4f(z) (z^{2} z_{*}^{6} h(z)^{3} h(z_{*}) - z^{6} z_{*}^{2} h(z) h(z_{*})^{3})^{3}}} \, \mathrm{d}z \right],$$

$$\frac{\mathrm{d}\ell}{\mathrm{d}z_{*}} = \frac{2z_{*}^{2}}{\sqrt{h(z_{*})}} \left[\lim_{z \to z_{*}} \frac{1}{\sqrt{z_{*}^{4} - z^{4} \frac{h(z_{*})^{2}}{h(z)^{2}}}} \frac{1}{\sqrt{f(z_{*})}} + z_{*}^{4} h(z_{*})^{2} \int_{0}^{z_{*}} \sqrt{\frac{4z^{10} h(z)^{6} (2h(z_{*}) - z_{*} h'(z_{*}))^{2}}{4f(z) (z^{2} z_{*}^{6} h(z)^{3} h(z_{*}) - z^{6} z_{*}^{2} h(z) h(z_{*})^{3})^{3}}} \, \mathrm{d}z \right].$$
(3.3)

Here, we also used the relation

$$U(z_*) = \int_{\epsilon}^{z_*} H(z, z_*) dz \longrightarrow \frac{dU(z_*)}{dz_*} = H(z_*, z_*) + \int_{\epsilon}^{z_*} \partial_{z_*} H(z, z_*) dz.$$
 (3.4)

3.2 Reconstruction formula

To leverage Bilson's method effectively, it is beneficial to choose the following coordinate

$$h(z) = 1. (3.5)$$

We will address the general case where $h(z) \neq 1$ towards the conclusion of this subsection.

Reconstruction formula I. Subsequently, we can recast the entanglement entropy (2.4) into the form

$$\frac{2G_N}{L^2\Omega} \frac{S(z_*)}{z_*^2} = \int_{\epsilon}^{z_*} \frac{1}{\sqrt{z_*^4 - z^4}} \frac{\sqrt{1/f(z)}}{z^2} dz.$$
 (3.6)

By comparing (3.1) and (3.6), we can establish

$$F(z_*) := \frac{2G_N}{L^2 \Omega} \frac{S(z_*)}{z_*^2}, \qquad Y(z) := \frac{\sqrt{1/f(z)}}{z^2}, \qquad G(z) := z^4, \tag{3.7}$$

and determine the "Solution" in (3.1) as

$$\sqrt{\frac{1}{f(z)}} = \frac{8G_N}{\pi L^2 \Omega} z^2 \frac{\mathrm{d}}{\mathrm{d}z} \int_{\epsilon}^{z} \frac{z_*}{\sqrt{z^4 - z_*^4}} S(z_*) \, \mathrm{d}z_*, \qquad (3.8)$$

together with (3.2) as

$$\frac{\mathrm{d}S(\ell)}{\mathrm{d}\ell} = \frac{L^2\Omega}{4G_N} \frac{1}{z_z^2} \,. \tag{3.9}$$

The resulting expression (3.8) represents the reconstruction formula provided by Bilson [44], where $S(z_*)$ is derived from the data $S(\ell)$, with ℓ interchangeable with z_* through (3.9). Essentially, given the entanglement entropy $S(\ell)$, the metric component f(z) can be generated as the output.

Reconstruction formula II. Although (3.8) presents a novel approach, the entanglement entropy data $S(\ell)$ predominantly hinges on the UV cutoff ℓ . Hence, from a practical standpoint, it proves beneficial [57] to employ an alternative reconstruction formula derived from the subsystem size in (2.4). Analogous to the entanglement entropy scenario, employing (3.1) yields:

$$\sqrt{\frac{1}{f(z)}} = \frac{2}{\pi} \frac{1}{z^2} \frac{\mathrm{d}}{\mathrm{d}z} \int_0^z \frac{z_*^3}{\sqrt{z^4 - z_*^4}} \ell(z_*) \, \mathrm{d}z_* \,, \tag{3.10}$$

where $\ell(z_*)$ serves as the input and f(z) emerges as the output.

However, it is noteworthy that the input data $\ell(z_*)$ essentially derives from (3.9), where the entanglement entropy $S(\ell)$ is provided. Thus, this second reconstruction formula (3.10) also represents a scenario where the input data is the entanglement entropy.

Example: pure AdS geometry. To illustrate how the reconstruction formula works, we consider an example where the analytic expression for the entanglement entropy is available. For the pure AdS geometry by

$$f(z) = 1, (3.11)$$

the entanglement entropy (2.4) can be analytically obtained as

$$S = S_{\text{CFT}} = \frac{L^2 \Omega}{2G_N} \left[\frac{1}{\epsilon} - \frac{2\pi}{\ell} \left(\frac{\Gamma\left(\frac{3}{4}\right)}{\Gamma\left(\frac{1}{4}\right)} \right)^2 \right] . \tag{3.12}$$

As the initial step of Bilson's method, we can first put the given the entanglement entropy from (3.12) into (3.9) and find $\ell(r_*)$

$$\ell(z_*) = \frac{2\sqrt{\pi} \Gamma\left(\frac{3}{4}\right)}{\Gamma\left(\frac{1}{4}\right)} z_*. \tag{3.13}$$

Then, by plugging this expression into the reconstruction formula (3.10), we can deduce

$$f(r) = 1, (3.14)$$

which aligns with (3.11).

Limitation of Bilson's method. Now we discuss the limitations of Bilson's method. It is straightforward to find that for the generic metric where

$$h(z) \neq 1, \tag{3.15}$$

Bilson's reformulation formulas, (3.10) and (3.2), become

$$\sqrt{\frac{1}{f(z)h(z)^3}} = \frac{2}{\pi} \frac{1}{z^2} \frac{\mathrm{d}}{\mathrm{d}z} \int_0^z \frac{\ell(z_*)}{\sqrt{\frac{z^4}{h(z)^2} - \frac{z_*^4}{h(z_*)^2}}} \frac{2z_*^3 h(z_*) - z_*^4 h'(z_*)}{2h(z_*)^3} \, \mathrm{d}z_*,
\frac{\mathrm{d}S}{\mathrm{d}\ell} = \frac{L^2 \Omega}{4G_N} \frac{h(z_*)}{z_*^2}.$$
(3.16)

Then, one can notice that the reconstruction program cannot proceed due to the inconsistency between the number of input data and output data. In other words, given a single data $S(\ell)$, one needs to determine two functions f(z) and h(z). Therefore, unless h(z) is provided, Bilson's method cannot fully reconstruct the metric.

Nevertheless, this limitation is not surprising, as previously noted [44]. Interestingly, in an alternative coordinate defined by:

$$ds^{2} = \frac{L^{2}}{r^{2}} \left[-g(r)e^{-\chi(r)}dt^{2} + \frac{dr^{2}}{g(r)} + (dx^{2} + dy^{2}) \right],$$
 (3.17)

the reconstruction formula is given by

$$\sqrt{\frac{1}{g(r)}} = \frac{2}{\pi} \frac{1}{r^2} \frac{\mathrm{d}}{\mathrm{d}r} \int_0^r \frac{r_*^3}{\sqrt{r^4 - r_*^4}} \, \ell(r_*) \, \mathrm{d}r_*,
\frac{\mathrm{d}S}{\mathrm{d}\ell} = \frac{L^2 \Omega}{4G_N} \frac{1}{r_*^2}.$$
(3.18)

Even if we reconstruct g(r) from the given $S(\ell)$ using (3.18), we still cannot determine the remaining metric component $\chi(r)$ in (3.17).

As advertised in the introduction, in the next section, we will show that utilizing the machine learning method, we can overcome the limitation of Bilson's method, i.e., one can reconstruct both f(z) and h(z) from the given $S(\ell)$.

3.3 Example: Linear-axion model

Despite the limitations that Bilson's method may entail, it remains a novel approach for constructing the blackening factor f(z). We conclude this section by considering an example where bulk reconstruction via Bilson's method is viable: when h(z) = 1.

In this context, we investigate the bulk reconstruction process when the entanglement entropy is provided numerically. To the best of our knowledge, our study represents the inaugural exploration of the numerical evaluation of the reconstruction formula (3.10).

Linear-axion model. For this purpose, we consider the linear-axion model [100], characterized by the action:

$$S = \int d^4x \sqrt{-g} \left(R + 6 - \frac{1}{4}F^2 - \frac{1}{2} \sum_{I=1}^2 (\partial \psi_I)^2 \right), \qquad (3.20)$$

where the field strength is F = dA. We set units $16\pi G_N = L = \Omega = 1$ for simplicity hereafter. Within the metric (2.1), the equations of motion from (3.20) allows the analytic

$$r = \frac{z}{\sqrt{h(z)}}, \quad g(r) = \left(1 - \frac{zh'(z)}{2h(z)}\right)^2 f(z), \quad \chi(r) = \log\left[\left(1 - \frac{zh'(z)}{2h(z)}\right)^2 h(z)\right]. \tag{3.19}$$

⁹The metric (3.17) can be derived from our ansatz (2.1) through the coordinate transformation:

background solutions as

$$f(z) = 1 - \frac{\beta^2}{2}z^2 - \left(1 - \frac{\beta^2}{2} + \frac{\mu^2}{4}\right)z^3 + \frac{\mu^2}{4}z^4,$$

$$A = \mu (1 - z) dt, \qquad \psi_I = \beta(x, y),$$
(3.21)

where the event horizon is set $z_h = 1$, μ is the chemical potential, and β the strength of broken translations.

It is noteworthy that axion theories [100–102] have proven valuable in studying strongly coupled condensed matter systems [103–108] through analyses involving conductivity [109–119], transport coefficients [120–140], and the collective dynamics of strongly coupled phases [114, 141–159, 159]. Additionally, they have been explored in quantum information applications [34, 160–165] and the application of the AdS/Deep learning correspondence [80].¹⁰

It is worth noting that [80] successfully generated the metric of linear-axion models based on given boundary optical conductivity data using a machine learning method. Here, we aim to demonstrate that the reconstruction formula (3.10) can yield the same bulk metric obtained from the machine learning method [80]. To accomplish this, we utilize the same parameter set employed in [80]:

$$(\mu, \beta) = \begin{cases} (0.5, 0.5), & (\text{Data 1}) \\ (0.5, 1.0), & (\text{Data 2}) \\ (1.0, 1.5). & (\text{Data 3}) \end{cases}$$
 (3.22)

Holographic entanglement entropy. Plugging (3.21) into (2.4), one can numerically evaluate the entanglement entropy. Nevertheless, due to the UV divergence, it is advantageous to examine its finite piece, denoted as S_{Finite} , given in (2.5).

Considering the parameters provided in (3.22), we illustrate S_{Finite} in Fig. 2.¹¹ Then, to utilize the numerically evaluated entanglement entropy S_{Finite} as the input data for Bilson's method, we employ the power-law fitting curve

$$S_{\text{Finite}} = \sum_{i=-1}^{c_{\text{max}}} c_i \ell^i, \qquad (3.23)$$

where we set $c_{\text{max}} = 5$ in this paper. For instance, we find that the numerically obtained S_{Finite} is matched with the fitting coefficients given in Table. 1. Note that the value of c_{-1} originates from the finite piece of pure AdS geometry (3.12):

$$-2\pi \left(\frac{\Gamma\left(\frac{3}{4}\right)}{\Gamma\left(\frac{1}{4}\right)}\right)^2 \approx -0.71777. \tag{3.24}$$

Additionally, $c_0 \approx 0$ aligns with the analytic examination of the small ℓ limit analysis of entanglement entropy for the linear-axion model, as provided in [34].

¹⁰Therefore, in this regard, our investigation into the linear-axion model (3.20) can be viewed as the bulk reconstruction of toy models for holographic strongly coupled materials within Bilson's method for the first time.

¹¹Strictly speaking, the corresponding entanglement entropy is $S_{\text{Finite}} z_h$ and ℓ/z_h .

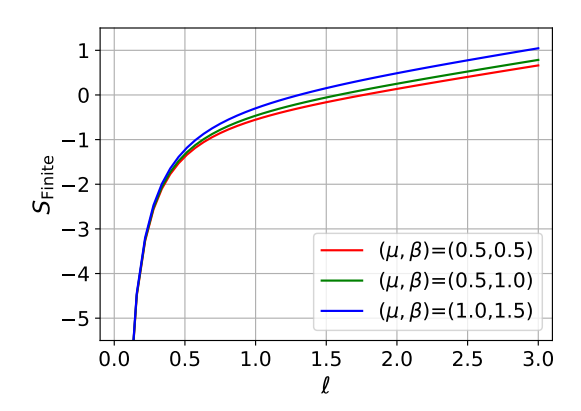


Figure 2. The finite piece of the entanglement entropy of linear-axion models when (μ, β) = Data 1 (red), Data 2 (green), Data 3 (blue): see (3.22). The numerically obtained S_{Finite} is aligned with the fitting (3.23) with the coefficients in Table. 1.

	c_{-1}	c_0	c_1	c_2	c_3	c_4	c_5
Data 1	-0.71778	0.00109	0.03538	0.15593	-0.03102	0.00320	-0.00012
Data 2	-0.71777	0.00041	0.17841	0.08822	-0.01526	0.00151	-0.00063
Data 3	-0.71775	-0.00084	0.41694	0.00291	-0.00039	0.00032	-0.00002

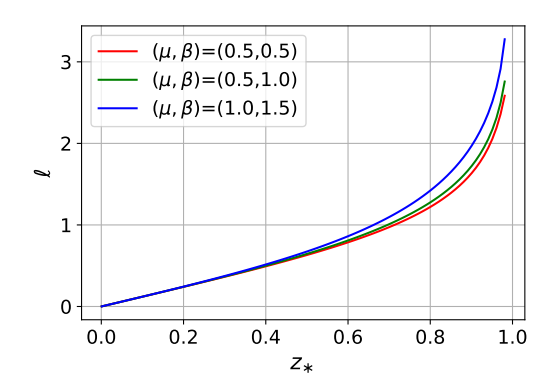
Table 1. Numerical fitting coefficients for (3.23) of the linear-axion model.

Bilson's method and bulk reconstruction. Now that we have the expression of S_{Finite} from (3.23), we can determine the entanglement entropy S using (2.5). Subsequently, similar to the pure AdS example in (3.11), the next step for Bilson's method entails inserting the numerically obtained S into the reconstruction formula (3.9) to determine $\ell(z_*)$. However, in this instance, we numerically evaluate $\ell(z_*)$ (as illustrated in the left panel of Fig. 3) and subsequently determine the bulk metric component f(z) numerically via the reconstruction formula (3.10).

The resulting f(z) from Bilson's method is depicted by the solid line in the right panel of Fig. 3. We confirm that this f(z) successfully reconstructs the target metric f(r) specified in (3.21). Therefore, our findings demonstrate that the metric of the linear-axion model can be constructed not only via the machine learning method utilizing optical conductivity [80], but also through Bilson's method (3.10) with entanglement entropy.

4 Machine learning method

In this section, we investigate bulk reconstruction employing the machine learning approach, which plays a pivotal role in revealing the complete metric described in (2.1). Our analysis demonstrates that by implementing machine learning techniques, we can overcome the constraints inherent in Bilson's method: specifically, we achieve the reconstruction of both f(z) and h(z) from the provided $S(\ell)$.



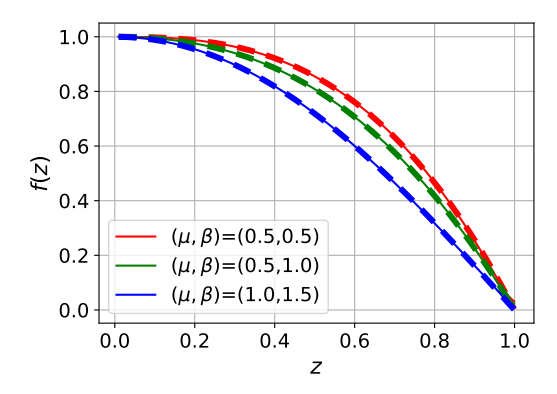


Figure 3. The subsystem size $\ell(z_*)$ (left panel) and the blackening factor f(z) (right panel) when $(\mu, \beta) = \text{Data 1 (red)}$, Data 2 (green), Data 3 (blue). The solid line is the one from Bilson's method (3.9) or (3.10), while the dashed line is f(z) in (3.21).

4.1 Methodology: Neural ODEs and Monte-Carlo integration

As discussed in the introduction, the machine learning holography framework, also known as the AdS/DL correspondence, has been employed in elucidating the holographic bulk theory that underpins quantum systems on the boundary.

In the pioneering studies of the AdS/DL correspondence [66, 67], significant advancements have primarily been achieved by *discretizing* the holographic bulk metric using deep learning techniques. For example, the ordinary differential equation (ODE) can be solved within the framework of a residual neural network (ResNet) [166], which is composed of residual blocks [167].

In recent years, to achieve a *continuous* holographic bulk spacetime, a continuous version of ResNet, known as the neural ordinary differential equation (neural ODE) [168], has been developed. By employing neural ODEs in machine learning holography, the continuous bulk metric has been reconstructed using boundary data, as demonstrated in the contexts of quantum chromodynamics [72] and strongly interacting condensed matter systems [80, 81].

Neural ODEs. In this paper, we utilize the neural ODE framework within the context of the holographic study of quantum information, with a particular focus on entanglement entropy. Our machine learning methodology represents an integrated version of the neural ODE, which we refer to as neural integration.

First, let us briefly review the concept of the ResNet using a simple ODE example:

$$\partial_z \mathcal{F} = \mathcal{G}(z, \mathcal{F}; \theta(z)),$$
 (4.1)

where \mathcal{F} is the unknown function of z, \mathcal{G} is a given function. Here, $\theta(z)$ represents a general hidden function within the ODE, which serves as the trainable parameters in the neural network. This equation can be solved using ODE solvers by discretizing the z interval into small steps Δz . For example, if we choose the Euler method as the solver, the approximate

numerical solution \mathcal{F}_N is given by

$$\mathcal{F}_N = \mathcal{F}_1 + \sum_{n=1}^{N-1} \mathcal{G}(z_n, \mathcal{F}_n; \theta_n) \cdot \Delta z, \qquad (4.2)$$

where the z interval is discretized into N steps, and \mathcal{F}_1 is the given initial value at z_1 (for more details, see [80]). Due to this discretization, the training parameters are also discretized; for instance, $\theta_n(z_n)$ could be the discretized metric $f_n(z_n)$. This is the fundamental concept of ResNet for generating the discretized bulk metric [66, 67].

The approximate numerical solution \mathcal{F} can be more generally expressed as:

$$\mathcal{F}_{\text{final}} = \text{ODE Solver} \left[\mathcal{G}; \, \mathcal{F}_{\text{initial}}, \, (z_{\text{final}}, \, z_{\text{initial}}); \, \theta(z) \right] \,.$$
 (4.3)

For instance, for the Euler method described in (4.2), we have

$$(\mathcal{F}_{\text{initial}}, \mathcal{F}_{\text{final}}) = (\mathcal{F}_1, \mathcal{F}_N) \text{ and } (z_{\text{initial}}, z_{\text{final}}) = (1, N - 1),$$
 (4.4)

with the training parameter θ chosen as θ_n for the ResNet.

To ensure that the discrete hidden function becomes a continuous function, the central idea of neural ODEs [168] is to replace the discrete parameter $\theta(z) = \theta_n(z_n)$ with a continuous deep neural network $\theta(z) = D(z)$. This deep neural network consists of multiple layers through which data is processed, including an input layer, several hidden layers, and an output layer.

The deep neural network is defined as follows

$$D(z) = W_M \cdot \phi(\cdots \phi(W_2 \cdot \phi(W_1 z + b_1) + b_2) \cdots) + b_M, \qquad (4.5)$$

where ϕ is an activation function, W_M is the weight matrix of M-th layer, and b_M is the bias vector of M-th layer. The activation function is a non-linear function applied to the output of each layer, enabling the network to model complex patterns. In this paper, we use the rectified linear unit (ReLU) as the activation function: ReLU(z) = max(0, z). The other parameters (weights and biases) are adjusted during training to minimize errors in the loss function.

Continuous training variables in deep neural networks, primarily weights and biases, are essential for the learning process. Weights determine the "strength" of connections between nodes, while biases provide each layer with a trainable constant value to help the model fit the data better. For an illustrative sketch of a deep neural network, see Fig. 4, which shows the case of 3 hidden layers with 3 nodes each. By employing iterative forward and backward propagation steps, along with optimization algorithms, these variables are continuously refined to minimize errors and enhance the model's efficacy.

In our deep neural network computations, we utilize the PyTorch framework [169], an open-source machine learning library, and deep neural networks are initialized with 3 hidden layers, each containing 20 nodes.

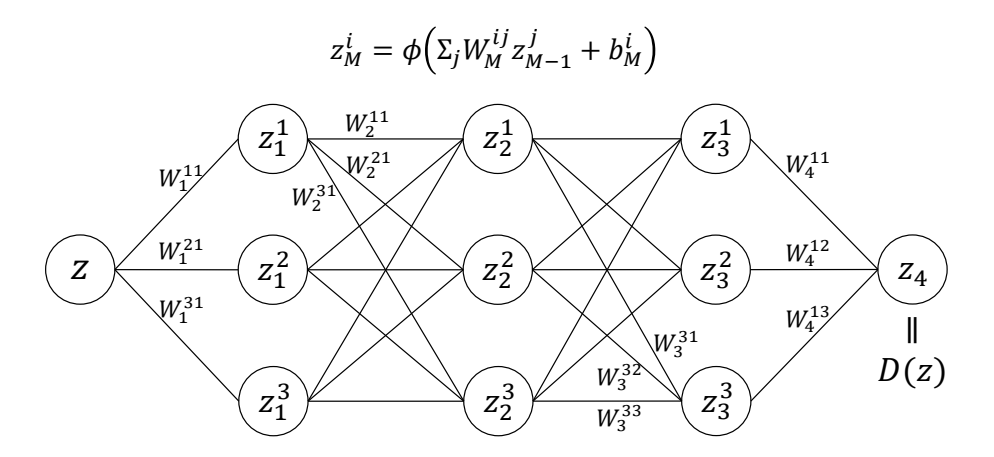


Figure 4. A structure of a deep neural network. It consists of 3 hidden layers with 3 nodes each. The nodes are fully connected each other. Through the learning procedure, the continuous function D(z) is generated where the input is $z =: z_0^1$.

Neural integrations. In this manuscript, drawing inspiration from solving ODEs using deep neural networks, we introduce a method for solving integrations through machine learning techniques. Termed "neural integration," this approach aligns well with our objective: employing machine learning holography to analyze entanglement entropy (2.5).

To demonstrate further, let us consider the following integration, which can be obtained by equation (4.1):

$$\mathcal{F} = \int_{z_{\text{initial}}}^{z_{\text{final}}} \mathcal{G}(z; D(z)) dz, \qquad (4.6)$$

where we substitute $\theta(z)$ with the deep neural network D(z). Subsequently, our primary objectives, the subsystem size ℓ (2.4), and the (finite piece) entanglement entropy S_{Finite} (2.5), can be expressed in the form of (4.6) as

$$S_{\text{Finite}} = \int_0^{z_*} \mathcal{G}_S(z; f(z), h(z)) \, dz - \frac{1}{z_*}, \qquad \ell = \int_0^{z_*} \mathcal{G}_\ell(z; f(z), h(z)) \, dz, \qquad (4.7)$$

where S_{Finite} (and ℓ) is compared with \mathcal{F} , and the metric components with the deep neural network D(z) in (4.5), i.e.,

$$f(z) \longleftrightarrow D_f(z), \qquad h(z) \longleftrightarrow D_h(z).$$
 (4.8)

The optimization of deep neural networks conducts through the learning process to achieve convergence between the estimated and intended values (given the input dataset S_{Finite} and ℓ). The estimated value is obtained via numerical integration in (4.7). In this study, Monte Carlo integration serves as the numerical integrator, with Torchquad [170], an extension package of PyTorch, utilized for Monte Carlo integration.¹²

¹²It is noteworthy that while bulk holographic geometry is derived from given entanglement entropy using deep learning methods [77, 78], the authors in [77] adopt ResNet together with the Runge-Kutta method within the ODE framework (4.1), ensuring that the emergent metric remains a discrete function. Using the different machine learning method based on the transformer algorithm, the discrete metric is also generated in [78].

More on the setup for machine learning holography. We further elaborate on the setup for our machine learning methodology. Instead of utilizing (4.8), we adopt the following technically convenient metric ansatz:

$$f(z) = (1-z) \left[1 + (a+1)z - z^2 D_f(z) \right], \qquad h(z) = 1 + az - z^2 D_h(z).$$
 (4.9)

This choice is motivated by several reasons. Firstly, we impose the horizon condition at the horizon (z = 1) as f(1) = 0, and the asymptotic AdS boundary condition at the boundary (z = 0) as f(0) = h(0) = 1. Furthermore, from the near-boundary expansion of $\mathcal{G}_S(z; f(z), h(z))$ in (4.7) together with (2.5), it follows that

$$\mathcal{G}_S(z; f(z), h(z)) \approx \frac{h'(0) - f'(0)}{z},$$
 (4.10)

which would result in a logarithmic UV divergence in S_{Finite} , which is assumed to be absent in our study.¹³ Within our ansatz (4.9), we eliminate this UV divergence since h'(0) = f'(0) = a. Essentially, within our ansatz (4.9), we have three training parameters in our machine learning method: the linear coefficient a, and the weights and biases of $D_f(z)$ and $D_h(z)$.

Then, substituting (4.9) into (4.7) and initializing random values for a, weights, and biases, $S_{\text{Finite}}(\ell)$ can be computed. As an intermediate numerical step, both $S_{\text{Finite}}(z_*)$ and $\ell(z_*)$ are evaluated within the selected range $z_* \in [0.1, 0.99]$.

Last but not least, we discuss the loss function L employed in our computation, which is defined as

$$L = \frac{1}{N_{\ell}} \sum_{\ell} \left| S_{\text{Finite}}^{(m)}(\ell) - S_{\text{Finite}}(\ell) \right| + \left| s^{(m)} - s \right|, \tag{4.11}$$

where N_{ℓ} denotes the number of the data points for ℓ . The first term quantifies the disparity between the output entanglement entropy data $S_{\text{Finite}}^{(m)}(\ell)$ computed by the machine learning and the provided input data $S_{\text{Finite}}(\ell)$. The second term, referred to as the penalty term, corresponds to the thermal entropy (s) (2.2), where the superscript index (m) indicates that the thermal entropy is obtained through machine learning. This term is important for shaping the loss function and influencing the the optimization process.

In principle, alternative penalty terms could be chosen. However, opting for the thermal entropy as the penalty term offers several intriguing aspects. Firstly, it aligns structurally with the first term in the loss function. In other words, $s^{(m)}$ is obtained through machine learning, while s is given from the input data. It is worth recalling that thermal entropy can be inferred from the large subsystem size limit as $S_{\text{Finite}} \approx s \, \ell$ [22, 62]. Furthermore, through the utilization of thermal entropy, an additional horizon condition on h(1) can be introduced via (2.2), complementing the demonstration provided below (4.9). Thus, in aggregate, we have imposed two AdS boundary conditions and two horizon condition on the metric components.

¹³Within the models of interest, we have checked that such an additional UV divergence term is absent.

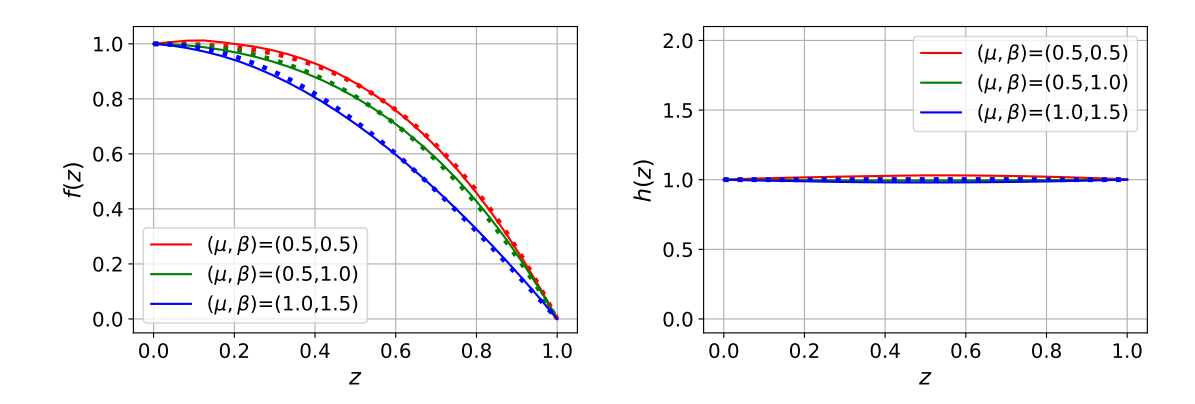


Figure 5. The emergent metric from the entanglement entropy of linear-axion model with the given dataset (3.22). Solid lines are the metric from machine learning method, while dotted lines denote the true metric (3.21).

4.2 Emergent spacetime from holographic entanglement entropy

Utilizing the aforementioned machine learning methodologies, we commence with the training procedure. Initially, within this section, we illustrate the emergence of full spacetime from holographic entanglement entropy. To achieve this, we employ two exemplary and extensively researched toy models of holographic matters, namely the Gubser-Rocha model [92] and holographic superconductor model [93, 94], where the former has been instrumental in examining the properties of strange metals. Our analysis here aims to demonstrate the machine learning's capability in accurately discerning the metric (2.1) based on holographic entanglement entropy.

4.2.1 Linear-axion model

As a warm-up, we verify the efficacy of our machine learning approach in scenarios where h(z) = 1, consistent with the results obtained through Bilson's method outlined in Sec. 3.3: the linear-axion model (3.20).

Within the same dataset (3.22), we input data derived from the holographic entanglement entropy of the linear-axion model into the machine learning framework. Recall the entanglement entropy depicted in Fig. 2, with fitting data represented by (3.23) and corresponding coefficients listed in table. 1.

In Fig. 5, we illustrate that our machine learning methodology successfully elucidates the black hole geometry f(z) within the holographic bulk spacetime. The emergent metric, as identified by the machine learning process, aligns closely with the geometry of the linear-axion model described by (3.21). In Appendix. B, we discuss the detailed discussion of the training procedure employed in our machine learning method, together with the error estimation analysis.

4.2.2 Gubser-Rocha model

Subsequently, we apply the machine learning methodology to the Gubser-Rocha model [92] where the metric component now $h(z) \neq 1$. Its action is defined as follows

$$S = \int d^4x \sqrt{-g} \left(R + 6 \cosh \phi - \frac{1}{4} e^{\phi} F^2 - \frac{3}{2} (\partial \phi)^2 - \frac{1}{2} \sum_{I=1}^2 (\partial \psi_I)^2 \right), \tag{4.12}$$

where $16\pi G_N = L = 1$. Here, ϕ represents the dilaton field, the field strength is $F = \mathrm{d}A$, and the axion field ψ_I is also included. Notably, the Gubser-Rocha model (4.12) stands out as one of the most prominent and celebrated holographic models, pivotal in elucidating the properties of strange metals. Remarkably, the Gubser-Rocha model facilitates the study of linear-in-T resistivity, attributed to the nature of the infrared fixed point [109, 110, 112, 116, 118, 119, 129, 138, 171–173].

The Gubser-Rocha model (4.12) possesses another attractive feature in that it allows for the analytic background solutions. Within our metric (2.1), it is described as

$$f(z) = (1-z)\frac{1+(1+3Q)z+(1+3Q(1+Q)-\frac{1}{2}\beta^2)z^2}{(1+Qz)^{3/2}}, \qquad h(z) = (1+Qz)^{3/2},$$
(4.13)

accompanied by the matter fields

$$A = (1 - z) \frac{\sqrt{3Q(1 + Q)\left(1 - \frac{\beta^2}{2(1 + Q)^2}\right)}}{1 + Qz} dt,$$

$$\phi = \frac{1}{2} \log[1 + zQ], \qquad \psi_I = \beta(x, y).$$
(4.14)

In these solutions, a free parameter, Q, is present. This parameter will be determined once the physical parameters, the chemical potential μ and the strength of momentum relaxation β , are given through

$$\mu := A_t(0) = \sqrt{3Q(1+Q)\left(1 - \frac{\beta^2}{2(1+Q)^2}\right)}, \qquad s = 4\pi\sqrt{(1+Q)^3},$$
(4.15)

where we also identify the thermal entropy s in (2.2) for our machine learning approach.

To initiate our machine learning methodology, we initially compute the holographic entanglement entropy. Since the Gubser-Rocha model entails two free parameters: (μ, β) , akin to the linear-axion model (3.20), we opt for the same dataset (3.22).

Subsequently, by substituting (4.13) into (2.5), one can compute the entanglement entropy numerically. Employing the parameters specified in (3.22), we depict S_{Finite} in Fig. 6, where we find its compatibility with (3.23) when fitted, with coefficients detailed in Table. 2.

 $^{^{14}}$ It is pertinent to note that the model also manifests characteristics relevant to high- T_c cuprate superconductivity, such as Homes's law in high- T_c superconductors [116, 173]. Furthermore, investigations into the phase diagram utilizing fermionic spectral functions [129] or conductivity [140] have been undertaken. Additionally, discussions on certain limitations in describing transport anomalies, such as the Hall angle, have also been addressed [119, 172].

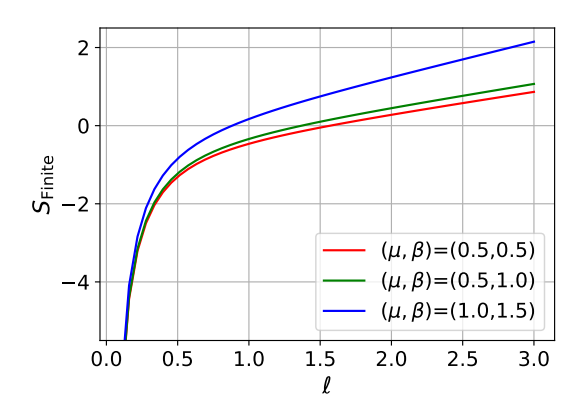


Figure 6. The finite piece of the entanglement entropy of Gubser-Rocha model when (μ, β) = Data 1 (red), Data 2 (green), Data 3 (blue): see (3.22). The numerically obtained S_{Finite} is aligned with the fitting (3.23) with the coefficients in Table. 2.

	c_{-1}	c_0	c_1	c_2	c_3	c_4	c_5
Data 1	-0.71778	0.06566	0.03271	0.19084	-0.04034	0.00441	-0.00018
Data 2	-0.71778	0.09288	0.17478	0.13203	-0.02557	0.00273	-0.00012
Data 3	-0.71776	0.35355	0.39487	0.17682	-0.04421	0.00700	-0.00047

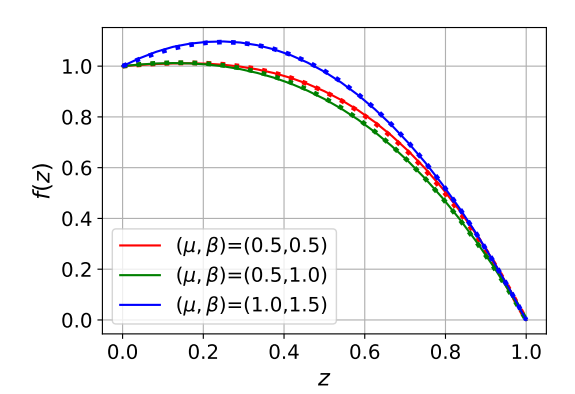
Table 2. Numerical fitting coefficients for (3.23) of Gubser-Rocha model.

It is worth noting that the value of c_0 for the Gubser-Rocha model is finite, unlike that for the linear-axion model as shown in Table. 1. To elucidate this distinction, we analytically investigate c_0 for our metric (2.1) in the limit of a small subsystems, as detailed in Appendix. A. Specifically, we examine c_0 as follows

$$c_0 = \frac{h'(0)}{2} \,. \tag{4.16}$$

We observe that when h(z) = 1, c_0 equals 0, consistent with the numerical findings in the linear-axion model. Conversely, when $h(z) \neq 1$, c_0 can be non-zero. This is evident in the case of the Gubser-Rocha model (4.13): we checked that our numerical results in Table. 2 align with the analytical formula (4.16).

Finally, we plug data obtained from the holographic entanglement entropy of the Gubser-Rocha model into the machine learning framework, utilizing the fitting data described by (3.23) and the corresponding coefficients outlined in Table. 2. Subsequently, in Fig. 7, we demonstrate that our machine learning methodology can reveal the complete black hole geometry f(z) and h(z) within the holographic bulk spacetime. This validation underscores the efficacy of our machine learning approach in capturing the entire geometry, even in scenarios where $h(z) \neq 1$. See also Appendix. B for the error estimation analysis of Gubser-Rocha model.



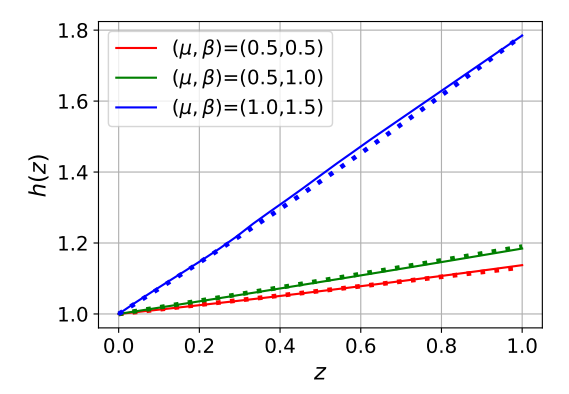


Figure 7. The emergent metric from the entanglement entropy of Gubser-Rocha model with the given dataset (3.22). Solid lines are the metric from machine learning method, while dotted lines denote the true metric (4.13).

4.2.3 Holographic superconductors

We proceed to discuss another prominent example of spacetime within holography, characterized by $h(z) \neq 1$, known as the holographic superconductor model [93, 94], often referred to as the HHH model after its proponents, Hartnoll, Herzog, and Horowitz. This model stands as one of the most widely studied frameworks in applied holography to condensed matter systems, garnering significant attention in the field (for comprehensive reviews, refer to [174, 175]).

Precisely speaking, the U(1) symmetry in the dual field theory of the HHH model is global rather than local, characterizing it as a superfluid rather than a superconductor. While some aspects, such as electric conductivity, may not distinguish between the two, other features, such as the dynamics of vortices and collective low-energy modes, markedly differentiate between a superfluid and a superconductor. For instance, collective excitations in holographic superfluids are second sound waves (superfluid Goldstone mode) [176, 177] which are absence in the superconductors. Explorations of collective excitations in holographic superconductors are conducted in [178], incorporating dynamical boundary gauge fields and explicitly confirming the Anderson-Higgs mechanism. Nevertheless, for the sake of consistency in our discussion, we continue to refer to the HHH model as representing holographic superconductors.

The HHH model [93, 94] is given as

$$S = \int d^4x \sqrt{-g} \left(R + 6 - \frac{1}{4} F^2 - |D\Phi|^2 - m^2 |\Phi|^2 \right), \tag{4.17}$$

where it composes of field strength F = dA and a complex scalar field Φ with the covariant derivative $D_{\mu}\Phi = (\nabla_{\mu} - iqA_{\mu})\Phi$, which is for superconducting phase. In this manuscript, we set $m^2 = -2$ and q = 3 as chosen in the original paper [93, 94].

To investigate the metric of holographic superconductors, we numerically solve the equations of motion derived from the action (4.17). For numerical convenience, we adopt

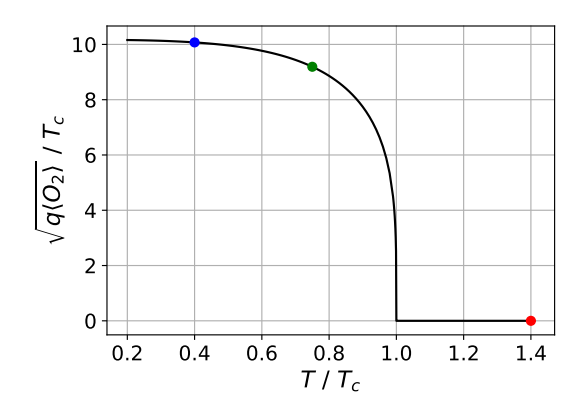


Figure 8. Condensation when $m^2 = -2$ and q = 3 where the critical temperature is $T_c/\mu = 0.156$. The dataset utilized for our machine learning analysis, (4.22), is denoted in (red, green, blue) dots.

the following ansatz for the metric

$$f(z) = (1 - z)U(z), h(z) = V(z),$$
 (4.18)

where we impose the boundary condition U(0) = V(0) = 1 to ensure the asymptotic AdS geometry. Additionally, for the matter fields, we choose

$$A = (1 - z)a(z) dt, \qquad \Phi = z \eta(z),$$
 (4.19)

Notably, the boundary behavior of these matter fields is characterized by

$$A_t = \mu - \rho z + \cdots, \qquad \Phi = \Phi^{(-)} z + \Phi^{(+)} z^2 + \cdots.$$
 (4.20)

According to the holographic dictionary, μ represents the chemical potential, ρ stands for the charge density, and in the asymptotic form of Φ , $\Phi^{(-)}$ denotes the source while $\Phi^{(+)}$ represents the condensate. In our chosen ansatz (4.19), we straightforwardly derive the chemical potential μ as $\mu = a(0)$ and the source $\Phi^{(-)}$ as $\Phi^{(-)} = \eta(0)$.

Next, as the boundary condition for the superconducting phase, we set the source to be zero, $\Phi^{(-)} = 0$, to describe the spontaneous symmetry breaking, expressed as

$$\Phi^- = 0, \quad \text{and} \quad \langle \mathcal{O}_2 \rangle := \sqrt{2} \, \Phi^+, \tag{4.21}$$

where the factor of $\sqrt{2}$ in defining the condensate $\langle \mathcal{O}_2 \rangle$ follows from [93], serving as a convenient normalization. Therefore, essentially, using the numerically obtained solutions, one can discern between the superconducting phase, characterized by $\Phi^{(+)} \neq 0$, and a normal phase, where $\Phi = 0$, by computing the temperatures using (2.2). We present the plot of the condensate in Fig. 8, depicting condensation when $m^2 = -2$ and q = 3, with a critical temperature of $T_c/\mu = 0.156$, consistent with findings in [94].

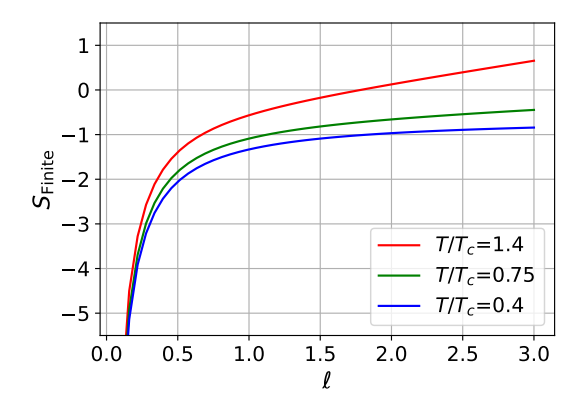


Figure 9. The finite piece of the entanglement entropy of superconductor model when $T/T_c = 1.4, 0.75, 0.4$ (red, green, blue). The numerically obtained S_{Finite} is aligned with the fitting (3.23) with the coefficients in Table. 3.

Similarly to the Gubser-Rocha model, we begin our machine learning methodology by computing the holographic entanglement entropy. For the superconductor examples, we select three representative datasets characterized by

$$T/T_c = (1.4, 0.75, 0.4),$$
 (4.22)

illustrated as colored dots in Fig. 8. Subsequently, by substituting the obtained numerical metric solutions (4.18) into (2.5), we compute the entanglement entropy, as shown in Fig. 9. We find its agreement with (3.23) when fitted, with coefficients provided in Table 3. Here,

	c_{-1}	c_0	c_1	c_2	c_3	c_4	c_5
$T/T_c = 1.4$	-0.71778	0.00317	-0.00981	0.20193	-0.05115	0.00716	-0.000397
$T/T_c = 0.75$	-0.71774	-0.40853	0.01507	0.02504	-0.00345	0.00033	-0.000013
$T/T_c = 0.4$	-0.71771	-0.63160	0.02676	-0.01275	0.00304	-0.00026	0.000001

Table 3. Numerical fitting coefficients for (3.23) of superconductor model.

we also confirmed that the analytical formula (4.16) yields consistent numerical values for c_0 in the superconductor model.

Finally, we incorporate data derived from the holographic entanglement entropy of the superconductor model into the machine learning framework. This involves utilizing the fitting data described by (3.23) along with the corresponding coefficients outlined in Table 3. Subsequently, in Fig. 10, we showcase how our machine learning methodology proficiently reveals the complete black hole geometry f(z) and h(z) for the holographic superconductor. This validation again underscores the effectiveness of our machine learning approach in accurately capturing the entire geometry, even in scenarios where $h(z) \neq 1$. The error estimation analysis for the holographic superconductor model is given in Appendix. B.

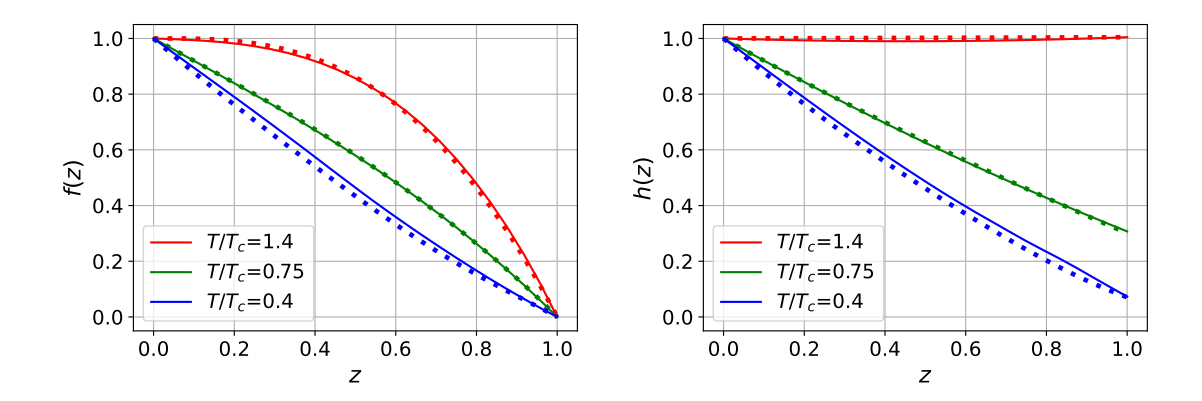


Figure 10. The emergent metric from the entanglement entropy of superconductor model. Solid lines are the metric from machine learning method, while dotted lines denote the true metric (4.18) obtained numerically solving equations of motion.

It is worth noting that the functional form of h(z) for superconductors differs from that of the Gubser-Rocha model (cfr. Fig. 10 vs. Fig. 7): h(z) monotonically decreases towards the horizon for superconductor models, unlike the Gubser-Rocha model. Nonetheless, we find that our machine learning approach can adeptly reconstruct all types of h(z).

4.3 Emergent spacetime from a one-dimensional chain

In this section, we demonstrate the applicability of deep learning in elucidating the emergent AdS spacetime from entanglement entropy data of many-body systems. For this purpose, we leverage data on the entanglement entropy of one-dimensional systems [98], specifically focusing on data from a fermionic tight-binding chain at half filling.

It is worth noting that [98] have also investigated the entanglement entropy in higherdimensional systems, which could be relevant to our AdS₄ setup (2.1). Nonetheless, unlike our holographic setup, the analysis in [98] does not consider strip-shaped entangling regions. Hence, in this section, we concentrate on the one-dimensional (1 + 1D) case.

4.3.1 Machine learning setup

Holographic setup. In order to study one-dimensional systems in holography, we consider the asymptotically AdS₃ spacetime as

$$ds^{2} = \frac{L^{2}}{z^{2}} \left[-f(z) dt^{2} + \frac{dz^{2}}{f(z)} + h(z) dx^{2} \right], \qquad (4.23)$$

where the corresponding temperature and thermal entropy read as

$$T = -\frac{f'(z)}{4\pi} \bigg|_{z_h}, \qquad s = \frac{L}{4G_N} \frac{\sqrt{h(z)}}{z} \bigg|_{z_h}.$$
 (4.24)

Then, within the metric (4.23), the holographic entanglement entropy S can be given [22, 62] as

$$S = \frac{L}{2G_N} \left[\int_{\epsilon}^{z_*} \frac{1}{z} dz + \int_{0}^{z_*} \frac{1}{z} \left(\sqrt{\frac{1}{1 - \frac{z^2}{z_*^2} \frac{h(z_*)}{h(z)}}} \frac{1}{\sqrt{f(z)}} - 1 \right) dz \right]$$

$$= \frac{L}{2G_N} \left[\log \left(\frac{1}{\epsilon} \right) + \left\{ \int_{0}^{z_*} \frac{1}{z} \left(\sqrt{\frac{1}{1 - \frac{z^2}{z_*^2} \frac{h(z_*)}{h(z)}}} \frac{1}{\sqrt{f(z)}} - 1 \right) dz + \log z_* \right\} \right]$$

$$:= \frac{L}{2G_N} \left[\log \left(\frac{1}{\epsilon} \right) + S_{\text{Finite}} \right],$$

$$(4.25)$$

together with the subsystem size ℓ

$$\ell = 2 \int_0^{z_*} \frac{1}{\sqrt{\frac{h(\alpha)}{h(z_*)} \frac{z_*^2}{\alpha^2} - 1}} \frac{1}{\sqrt{h(\alpha)f(\alpha)}} d\alpha.$$

$$(4.26)$$

Example: BTZ black holes and 1 + 1D CFT. One of the landmark outcomes in holographic entanglement entropy [22, 62] is the utilization of the Ryu-Takayanagi formula with BTZ black holes:

$$f(z) = 1 - z^2$$
, $h(z) = 1$, (4.27)

where $z_h = 1$, yielding the consistent entanglement entropy of a 1 + 1D CFT. Substituting (4.27) into (4.25)-(4.26), one derives

(BTZ black holes):
$$S = \frac{L}{2G_N} \log \left[\frac{2}{\epsilon} \sinh \left(\frac{\ell}{2} \right) \right], \quad \ell = 2 \operatorname{arctanh}(z_*).$$
 (4.28)

This aligns with the CFT result

$$S_{\text{CFT}} = \frac{c}{3} \log \left[\frac{\beta}{\pi \epsilon} \sinh \left(\frac{\pi \ell}{\beta} \right) \right],$$
 (4.29)

with the identification

$$c = \frac{3L}{2G_N}, \qquad \beta = \frac{1}{T} = 2\pi.$$
 (4.30)

where c represents the central charge and β stands for the inverse temperature derived via (4.24).

Setup for machine learning method. Building upon the holographic setup (4.25)-(4.26), next we discuss our machine learning setup for one-dimensional system. Especially, to leverage the data provided in [98], we introduce S_{DATA} as defined in [98],

$$S_{\text{DATA}} := S - \frac{c}{3} \log \left[\frac{\beta v}{\pi \epsilon} \right],$$
 (4.31)

where v is the group velocity, potentially varying across systems. Subsequently, comparing (4.31) with the holographic entanglement entropy S in (4.25), one can find the finite piece as

$$S_{\text{Finite}} = \frac{3}{c} S_{\text{DATA}} + \log\left(\frac{\beta v}{\pi}\right),$$
 (4.32)

employing $c = 3L/(2G_N)$. Essentially, by substituting the data S_{DATA} obtained from [98] into the right-hand side of equation (4.32), we can determine the metric on the left-hand side, namely the holographic formula (4.25).

Furthermore, in order to align with the data, we adopt the fitting curve for S_{DATA} as utilized in [98]:

$$S_{\text{DATA}} := \frac{c}{3} \log \left[\sinh \left(\frac{\pi \ell}{\beta v} \right) \right],$$
 (4.33)

where it is referred to as the universal scaling function.¹⁵ One comment is in order. By rescaling βv to β , one may eliminate the dependence on group velocity in the formula. However, we do not adopt this approach, as it has been reported that the group velocity may vary between different systems. Specifically, the group velocity can be calculated based on the lowest energy within the symmetry sector associated with the crystal momentum. For further discussion, refer to [98, 180].

4.3.2 Emergent metric from a fermionic tight-binding chain at half filling

As a supplementary note, it is worth mentioning the following. Let us consider the entanglement entropy S pertaining to the bipartition of a one-dimensional quantum many-body system into a subsystem of length ℓ . When the system parameters and energy (temperature) fall within a quantum critical regime of the model under consideration, established principles dictate that the entanglement entropy may adhere to a universal scaling function [181–183].

Notably, in [98], it has been demonstrated that for the typical quantum many-body systems complying with the eigenstate thermalization hypothesis, the entanglement entropy of eigenstates can be characterized by a universal scaling function. Particularly, in critical one-dimensional systems with linear dispersion at low energies, a universal scaling function follows from CFT.¹⁶

In this paper, within machine learning framework, we focus on analyzing data obtained from a fermionic tight-binding chain at half filling [98], where it has been demonstrated

¹⁵In principle, $S_{\rm DATA}$ may contain a non-universal constant, which does not affect the scaling behavior of ℓ and, therefore, is also not explicitly specified in [98]. Similarly, we omit such a term in our analysis. Notably, in the study of entanglement entropy, examining the derivative of S with respect to the spatial size of the entalgment region ℓ can prove advantageous. This approach, as suggested by [179], offers data that are unaffected by the UV cutoff, thereby also avoiding the appearance of a non-universal constant.

¹⁶The presence of gapless excitations can be indicative of a critical point. At this point, the system does not have a well-defined energy scale (gap) and exhibits critical fluctuations over all length scales. In a one-dimensional fermionic chain, the critical point manifests as a linear dispersion relation near the Fermi points $k = \pm \pi/2$ as $E(k) \approx v_F(k \mp \pi/2)$, leading to low-energy excitations where v_F is the Fermi velocity.

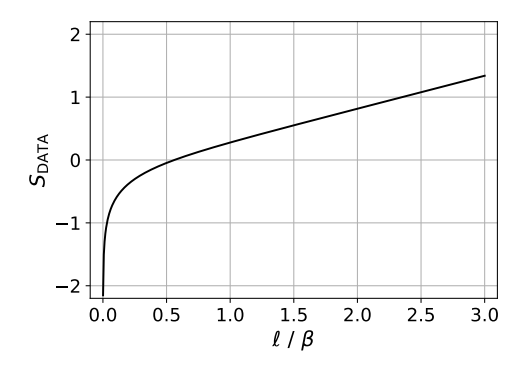


Figure 11. S_{DATA} for fermionic tight-binding chain at half filling [98], where (4.33) is used with (c, v) = (1, 2).

to adhere to the eigenstate thermalization hypothesis and is describable by a CFT with c=1. Notably, the entanglement entropy data S_{DATA} from this chain is found to be with parameters (c, v) = (1, 2) in (4.33): See Fig. 11.

Furthermore, in our machine learning method, for the sake of comparison, we also investigate the BTZ case (4.29). In essense, we have two datasets available:

$$(c, v, \beta) = \begin{cases} (24\pi, 1, 2\pi), & (BTZ case) \\ (1, 2, 1), & (Fermionic tight-binding chain at half filling) \end{cases}$$
(4.34)

where $c = 3L/(2G_N)$ with $L = 16\pi G_N = 1$ is employed for the BTZ case.¹⁷ Note that the data from [98], Fig. 11, is scaled with the inverse temperature β . This can be accommodated within the machine learning process by setting a fixed β ,

$$\beta = \frac{1}{T} = -\frac{4\pi}{f'(1)} := 1, \tag{4.35}$$

where (4.24) is utilized.

Last but not least, it is worth noting that in our machine learning method aimed at determining the complete metric, we utilize information of the thermal entropy s in (4.24). When dealing with data, obtaining such thermal entropy is straightforward, as it can be derived from the slope of the entanglement entropy in the large subsystem size limit [98]

$$(\ell \gg 1): \quad S \approx S_{\text{DATA}} \approx s \, \ell, \quad \longrightarrow \quad s = \frac{c\pi}{3\beta v},$$
 (4.36)

where we employ (4.33), which aligns with holography [22, 62].¹⁸ Intuitively, when $\ell \gg 1$ the subsystem effectively encompasses the entire system, implying that the minimal surface lies along the black hole horizon [45, 184], suggesting a potential connection between the

The combining (4.32) with (4.33), one can notice that c does not play any role in S_{Finite} . Nevertheless, we set $L = 16\pi G_N = 1$ and $\beta = 2\pi$ in order for the metric of the BTZ black hole (4.27). It is noteworthy that the central charge c can appear in our machine learning method through the thermal entropy (4.36).

¹⁸We also confirmed that the slop of the holographic entanglement entropy in the large ℓ limit, given in Fig. 2, 6, 9 are consistent with the thermal entropy from (2.2).

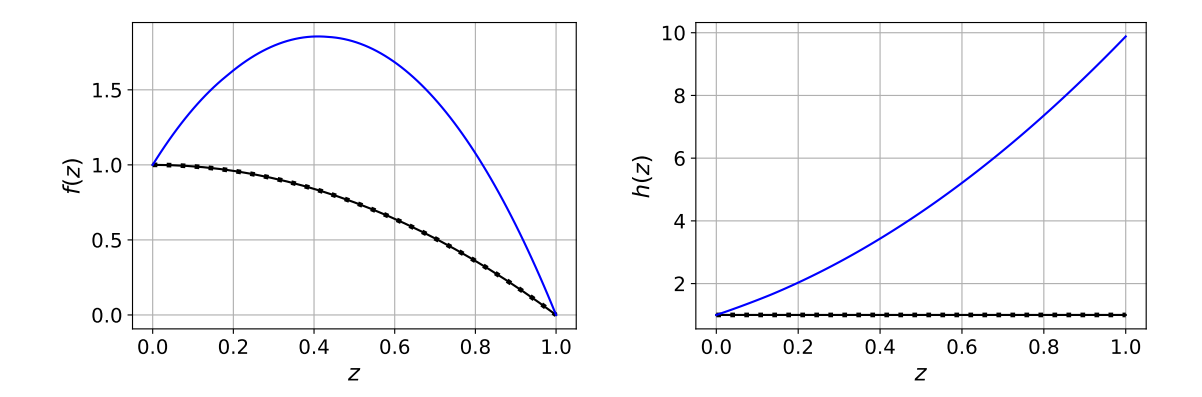


Figure 12. The emergent metric from the entanglement entropy of BTZ black holes (black data) and fermionic tight-binding chain at half filling (blue data). Solid lines are the metric from machine learning method, while dotted lines denote the true metric of BTZ black hole (4.27).

Ryu-Takayanagi formula (2.3) and the thermal entropy density s.

Finally, we utilize data obtained from the entanglement entropy of a fermionic tight-binding chain at half filling, as depicted in Fig. 11, into our machine learning framework. Subsequently, as illustrated in Fig. 12, we demonstrate how our machine learning method-ology adeptly uncovers the complete black hole geometry f(z) and h(z), even leveraging entanglement entropy data from quantum many-body systems.

Two noteworthy findings are made from our analysis. Firstly, as demonstrated in Fig. 12, our machine learning method accurately captures the dual geometry of the CFT, specifically in the BTZ case. This validation suggests that our approach can yield continuous geometries from the entanglement entropy of the CFT, representing an advancement beyond the machine learning analysis that produces discontinuous geometries of the BTZ black holes [77, 78].

Secondly, the functional form of the emergent metric derived from the fermionic tight-binding chain at half filling exhibits similar aspects to that of the Gubser-Rocha model: cfr. Fig. 7 vs. Fig. 12. The blackening factor f(z) attains a maximum value, forming a peak between the AdS boundary and the horizon, while, the function h(z) increases monotonically towards the horizon. This resemblance may not be surprising, as both models describe the metallic phases. In the Gubser-Rocha model, metallic behavior is characterized by the linear-temperature resistivity, whereas in the fermionic tight-binding chain, it is characterized by the gapless excitations.

We conclude this section by providing a heuristic and indicative argument for the peak structure of f(z) in the fermionic tight-binding chain at half-filling. According to holographic duality, the radial coordinate z in the bulk corresponds to the energy scale in the boundary theory. Thus, a peak at some z may be interpreted as indicating a significant energy scale in fermionic chain. This could represent the energy at which a density of states

(DOS) peak, indicating a high DOS at a particular energy level. For instance, DOS for a one-dimentional fermionic tight-binding model is given by $D(E) \approx 1/\sqrt{4t_h^2 - E^2}$, where t_h is the hopping parameter and E is the energy [185, 186].¹⁹ This form highlights the characteristic features of the DOS in such a system, indicating singularities at $E = \pm 2t_h$, known as Van Hove singularities.

In this context, we speculate that a peak structure in the AdS bulk, as depicted in Fig. 12, may be associated with features of a fermionic tight-binding chain at half-filling, particularly as the reminiscent of high DOS due to Van Hove singularities: $E = \pm 2t_h$ where $t_h = 1$ in our entanglement entropy data [98]. Nevertheless, the precise nature of this peak within the bulk direction remains insufficiently understood and is likely influenced by the specific properties of the tight-binding model under consideration as well. Therefore, our argument remains speculative and a more rigorous investigation with thorough analysis are required to attain a comprehensive understanding.

5 Conclusions

We have investigated the bulk reconstruction of the AdS black hole spacetime by leveraging quantum entanglement measures on the boundary field theory. Notably, by incorporating a neural network framework for the Ryu-Takayanagi formula within the AdS/DL correspondence, we introduce a machine learning approach to uncover the dual holographic emergent bulk metric from the entanglement entropy data of quantum many-body systems.

Our analysis of various entanglement entropy datasets within a continuous and generic metric configuration marks significant progress in the field of machine learning holography, both practically and theoretically. By employing the neural ODE methodology together with Monte-Carlo integration, our machine learning algorithm constructs a neural network from the entanglement entropy data, where the continuous network geometry represents the emergent holographic geometry of the quantum many-body state. Furthermore, our algorithm's ability to handle a generic metric ansatz (2.1) enhances its practical applicability, enabling the use of potential experimental and simulated quantum information data from strongly coupled field theories for gravity duals.

It is noteworthy to recall that our approach surpasses previous methods in machine learning holography with entanglement entropy, such as those in [77, 78], which exhibited inherent discontinuities in the reconstructed bulk metric with a simplified metric setup where h(z) = 1 in (2.1).

In our study, we initially utilized holographic entanglement entropy as input data for our machine learning approach. This enabled us to accurately derive the bulk metrics for both the Gubser-Rocha model and holographic superconductor models, which are prominent holographic models of strongly coupled quantum systems characterized by a non-trivial metric where $h(z) \neq 1$: see Fig. 7 for the case of Gubser-Rocha model and Fig. 10 for the superconductor model.

¹⁹Recall that the energy dispersion is $E(k) = -2t_h \cos k$ with k being the wavevector in the first Brillouin zone, typically $k \in [-\pi, \pi]$ for a one-dimensional chain. Then, DOS can be computed via $D(E) = \frac{1}{2\pi} \frac{dk}{dE}$.

Additionally, our machine learning approach successfully incorporates entanglement entropy data from a fermionic tight-binding chain at half filling in critical one-dimensional systems [98], and identifies the corresponding emergent bulk metric: see Fig. 12. Remarkably, we observed that the emergent metric exhibits a resemblance to that of the Gubser-Rocha model, where h(z) increases monotonically towards the horizon and f(z) reveals an anomalous peak structure. This resemblance may be attributed to the fact that both models can describe metallic phases, with the Gubser-Rocha model featuring linear-temperature resistivity and the fermionic tight-binding chain exhibiting gapless excitations, where electrons can move freely without encountering an energy gap.

Our successful results indicate that, on a practical level, our algorithm enhances the efficiency of modeling the emergent metric from the entanglement structure of quantum many-body systems. Furthermore, it signifies the successful completion of the bulk reconstruction program, thereby advancing our understanding of holographic emergent gravity derived from quantum entanglement.

It is noteworthy that much of the work on metric reconstruction, including our own, has been motivated by the idea that spacetime is constructed through entanglement entropy. However, it has been argued that "entanglement is not enough" to fully encode spacetime [187], as the Ryu-Takayanagi surface in the gravity context only probes the exterior metrics of black holes. To gain insight into the full geometry even interior of a black hole, it has been proposed that quantum computational complexity plays a crucial role. Indeed, based on various holographic complexity proposals, such as complexity=volume [187, 188], complexity=volume 2.0 [189], and complexity=anything [190], the internal metrics of black holes have been successfully reconstructed without employing machine learning techniques [56, 57].

In general, understanding the internal structure of a black hole poses a captivating and fundamental challenge, both theoretically and experimentally. A recent and actively studied direction in holography involves examining the structure and dynamics of the black hole interior, particularly near the singularity where spacetime curvature becomes infinitely intense. For instance, pioneering work on the Kasner singularity in holography can be found in [191].

As such, exploring and reconstructing the interior geometry of a black hole using machine learning holographic techniques is highly significant, not only from the perspective of quantum information theory via complexity but also for advancing the study of quantum gravity. We intend to pursue this line of research in future studies and plan to address it in subsequent investigations.

Acknowledgments

We would like to thank Yongjun Ahn, Juan F. Pedraza for valuable discussions and correspondence. This work was supported by the Basic Science Research Program through the National Research Foundation of Korea (NRF) funded by the Ministry of Science, ICT & Future Planning (NRF-2021R1A2C1006791) and the AI-based GIST Research Scientist

Project grant funded by the GIST in 2024. This work was also supported by Creation of the Quantum Information Science R&D Ecosystem (Grant No. 2022M3H3A106307411) through the National Research Foundation of Korea (NRF) funded by the Korean government (Ministry of Science and ICT). H.-S Jeong acknowledges the support of the Spanish MINECO "Centro de Excelencia Severo Ochoa" Programme under grant SEV-2012-0249. This work is supported through the grants CEX2020-001007-S and PID2021-123017NB-I00, funded by MCIN/AEI/10.13039/501100011033 and by ERDF A way of making Europe. B. Ahn was supported by Basic Science Research Program through the National Research Foundation of Korea funded by the Ministry of Education (NRF-2020R1A6A3A01095962, NRF-2022R1I1A1A01064342). All the authors contributed equally to this paper and should be considered as co-first authors.

A Entanglement entropy in the small subsystem size limit

In this section, we derive the holographic entanglement entropy (2.5) in the limit of small subsystem size $\ell \ll 1$ (or small z_*). In this regime, the Ryu-Takayanagi surface is located near the AdS boundary. Consequently, we consider the asymptotic AdS behavior of the metric (2.1) as follows

$$f(z) = 1 + f'(0)z + \cdots, \qquad h(z) = 1 + h'(0)z + \cdots,$$
 (A.1)

where f'(0) = h'(0) is the model-dependent constant. By substituting this expression for ℓ into (2.4) and expanding the integrand for small z_* , we find

$$\ell = z_* \frac{2\sqrt{\pi} \Gamma\left(\frac{7}{4}\right)}{3\Gamma\left(\frac{5}{4}\right)},\tag{A.2}$$

which holds for small ℓ . Similarly, utilizing (A.1) and (A.2), we can analytically compute the holographic entanglement entropy (2.5) in the small ℓ limit as

$$S_{\text{Finite}} = -\frac{2\pi}{\ell} \left(\frac{\Gamma\left(\frac{3}{4}\right)}{\Gamma\left(\frac{1}{4}\right)} \right)^2 + \frac{h'(0)}{2} + \cdots, \tag{A.3}$$

where \cdots denotes the $\mathcal{O}(\ell)$ correction, which can be obtained by considering the z^2 order in the metric in (A.1). Comparing (3.23) with (A.3), we can determine c_0 as (4.16).

B The procedure of training the network and the error estimation

In this section, we discuss the training procedure employed in our machine learning approach, along with the error estimation.

In Fig. 13 (a)-(c), we illustrate the representative results for the holographic models, namely, the linear-axion model, the Gubser-Rocha model, and the holographic superconductor model, using Data 2 from (3.22) and $T/T_c = 0.75$. The figure clearly demonstrates that throughout the training process, the metric functions f(z) and h(z) gradually converge towards the values (indicated by blue lines) obtained from the holographic models:

the gray lines represent the metric components initialized (i.e., before training) with random values on weights W^{ij} and biases b^i of the deep neural networks. Additionally, in Fig. 13 (d), we depict the training procedure for the tight-binding chain model.

In the figure, we also present both the untrained and trained entanglement entropy data for all the models under consideration. It is evident that the entanglement entropy calculated with the trained metrics, represented by blue dots, closely aligns with the input entanglement entropy data (depicted by the black solid line).

We also evaluate the loss function (4.11) estimated from our machine learning method. For all datasets, we find that the values of both the first and second terms in (4.11) consistently remain within the range of 10^{-4} to 10^{-2} after training: for instance, see Fig. 14 for the Gubser-Rocha model. It is expected that as these numerical values decrease further, for instance to the order of 10^{-10} , the error in our machine learning results (e.g., a small deviation in the blue data in Fig. 10) will correspondingly diminish.

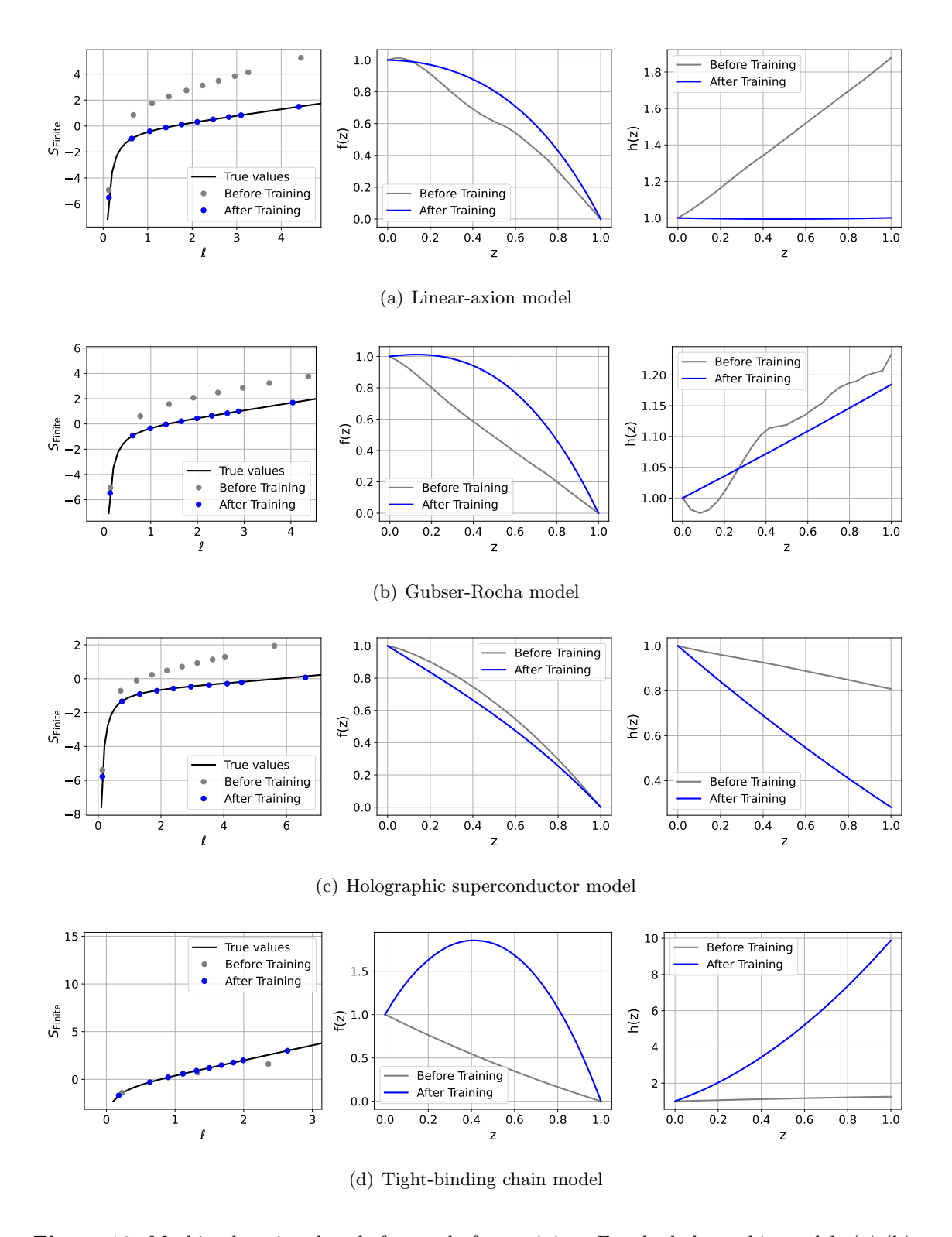


Figure 13. Machine learning data before and after training. For the holographic models (a)-(b), Data 2 from (3.22) is utilized, and $T/T_c = 0.75$ is for the model (c). In all figures, the gray data represents the results before training, whereas the blue data indicates the results after training. The black solid line in S_{Finite} represents the input entanglement entropy data.

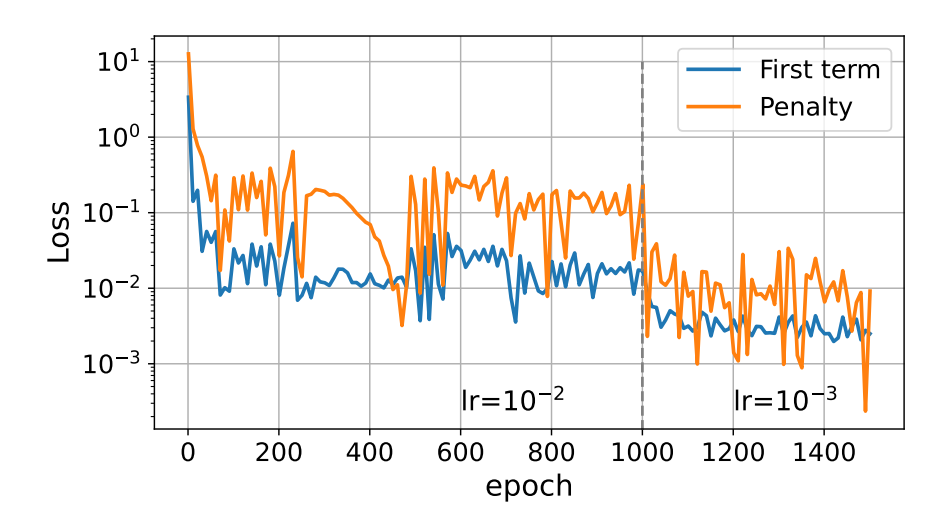


Figure 14. The first and second term of the Loss function (4.11) of Data 2 in the Gubser-Rocha model. The horizontal axis (epoch) denotes the number of updating the training parameters. The learning rate (lr) is set up by 10^{-2} before the 1000 epoch, and by 10^{-3} after that.

References

- [1] R. Horodecki, Quantum entanglement, Reviews of Modern Physics 81 (2009) 865–942.
- [2] A. Aspect, Bell's inequality test: more ideal than ever, Nature 398 (Mar., 1999) .
- [3] M. A. Nielsen and I. L. Chuang, <u>Quantum Computation and Quantum Information: 10th</u> Anniversary Edition. Cambridge University Press, June, 2012, 10.1017/cbo9780511976667.
- [4] L. Amico, Entanglement in many-body systems, Reviews of Modern Physics 80 (2008) 517–576.
- [5] P. Calabrese and J. Cardy, <u>Entanglement entropy and conformal field theory</u>, <u>J. Phys.</u> A42 (2009) 504005, [0905.4013].
- [6] T. Nishioka, S. Ryu and T. Takayanagi, <u>Holographic Entanglement Entropy: An Overview</u>,
 J. Phys. A42 (2009) 504008, [0905.0932].
- [7] R. Islam, R. Ma, P. M. Preiss, M. Eric Tai, A. Lukin, M. Rispoli et al., <u>Measuring</u> entanglement entropy in a quantum many-body system, Nature **528** (Dec., 2015).
- [8] N. Laflorencie, Quantum entanglement in condensed matter systems, Phys. Rept. **646** (2016) 1–59, [1512.03388].
- [9] J. Eisert, M. Cramer and M. Plenio, <u>Area laws for the entanglement entropy a review</u>, Rev. Mod. Phys. **82** (2010) 277, [0808.3773].
- [10] A. Kitaev and J. Preskill, <u>Topological entanglement entropy</u>, <u>Physical Review Letters</u> **96** (2006) .
- [11] M. Levin and X.-G. Wen, <u>Detecting Topological Order in a Ground State Wave Function</u>, <u>Phys. Rev. Lett.</u> **96** (2006) 110405, [cond-mat/0510613].
- [12] H. C. Jiang, Z. Wang and L. Balents, <u>Identifying topological order by entanglement entropy</u>, <u>Nature Phys.</u> 8 (2012) 902–905, [1205.4289].
- [13] Y. Zhang, T. Grover and A. Vishwanath, Entanglement entropy of critical spin liquids, Phys. Rev. Lett. **107** (2011) 067202, [1102.0350].
- [14] S. V. Isakov, M. B. Hastings and R. G. Melko, <u>Topological entanglement entropy of a bose-hubbard spin liquid</u>, Nature Physics **7** (2011) 772, [1102.1721].
- [15] G. Vidal, J. I. Latorre, E. Rico and A. Kitaev, <u>Entanglement in quantum critical phenomena</u>, <u>Phys. Rev. Lett.</u> 90 (2003) 227902, [quant-ph/0211074].
- [16] J. H. Bardarson, F. Pollmann and J. E. Moore, Unbounded Growth of Entanglement in Models of Many-Body Localization, Phys. Rev. Lett. 109 (2012) 017202.
- [17] A. J. Daley, H. Pichler, J. Schachenmayer and P. Zoller, Measuring Entanglement Growth in Quench Dynamics of Bosons in an Optical Lattice, Phys. Rev. Lett. 109 (2012) 020505.
- [18] N. Schuch, M. M. Wolf, F. Verstraete and J. I. Cirac, <u>Entropy Scaling and Simulability by Matrix Product States</u>, <u>Phys. Rev. Lett.</u> 100 (2008) 030504, [0705.0292].

- [19] E. Witten,

 Anti-de Sitter space, thermal phase transition, and confinement in gauge theories,

 Adv.Theor.Math.Phys. 2 (1998) 505–532, [hep-th/9803131].
- [20] S. S. Gubser, I. R. Klebanov and A. M. Polyakov, Gauge theory correlators from non-critical string theory, <u>Phys. Lett.</u> **B428** (1998) 105–114, [hep-th/9802109].
- [21] J. Maldacena, The large-n limit of superconformal field theories and supergravity, International Journal of Theoretical Physics 38 (Apr., 1999) 1113–1133.
- [22] S. Ryu and T. Takayanagi, <u>Holographic derivation of entanglement entropy from AdS/CFT</u>, <u>Phys. Rev. Lett.</u> 96 (2006) 181602, [hep-th/0603001].
- [23] V. E. Hubeny, M. Rangamani and T. Takayanagi, <u>A Covariant holographic entanglement entropy proposal</u>, <u>JHEP</u> **07** (2007) 062, [0705.0016].
- [24] T. Faulkner, A. Lewkowycz and J. Maldacena, Quantum corrections to holographic entanglement entropy, <u>JHEP</u> 11 (2013) 074, [1307.2892].
- [25] X. Dong, Holographic entanglement entropy for general higher derivative gravity, Journal of High Energy Physics **2014** (Jan, 2014) 44.
- [26] X. Dong, <u>The Gravity Dual of Renyi Entropy</u>, <u>Nature Commun.</u> 7 (2016) 12472, [1601.06788].
- [27] T. Takayanagi and K. Umemoto, Entanglement of purification through holographic duality, Nature Phys. 14 (2018) 573–577, [1708.09393].
- [28] P. Nguyen, T. Devakul, M. G. Halbasch, M. P. Zaletel and B. Swingle, <u>Entanglement of purification: from spin chains to holography</u>, <u>JHEP</u> 01 (2018) 098, [1709.07424].
- [29] S. Dutta and T. Faulkner, <u>A canonical purification for the entanglement wedge cross-section</u>, <u>JHEP</u> **03** (2021) 178, [1905.00577].
- [30] H.-S. Jeong, K.-Y. Kim and M. Nishida, Reflected Entropy and Entanglement Wedge Cross Section with the First Order Correction, JHEP 12 (2019) 170, [1909.02806].
- [31] M. Rangamani and T. Takayanagi, <u>Holographic Entanglement Entropy</u>. Springer International Publishing, 2017, 10.1007/978-3-319-52573-0.
- [32] A. B. Zamolodchikov,
 <u>Irreversibility of the Flux of the Renormalization Group in a 2D Field Theory</u>, <u>JETP Lett.</u>
 43 (1986) 730–732.
- [33] T. Albash and C. V. Johnson,

 <u>Holographic Studies of Entanglement Entropy in Superconductors</u>, <u>JHEP</u> **05** (2012) 079,

 [1202.2605].
- [34] H.-S. Jeong, K.-Y. Kim and Y.-W. Sun, <u>Holographic entanglement density for spontaneous symmetry breaking</u>, <u>JHEP</u> **06** (2022) 078, [2203.07612].

- [35] A. Hamilton, D. N. Kabat, G. Lifschytz and D. A. Lowe, <u>Holographic representation of local bulk operators</u>, <u>Phys. Rev. D</u> 74 (2006) 066009, [hep-th/0606141].
- [36] T. De Jonckheere, Modave lectures on bulk reconstruction in AdS/CFT, PoS Modave2017 (2018) 005, [1711.07787].
- [37] D. Harlow, TASI Lectures on the Emergence of Bulk Physics in AdS/CFT, Pos TASI2017 (2018) 002, [1802.01040].
- [38] N. Kajuri, <u>Lectures on Bulk Reconstruction</u>, <u>SciPost Phys. Lect. Notes</u> **22** (2021) 1, [2003.00587].
- [39] S. de Haro, S. N. Solodukhin and K. Skenderis, Holographic reconstruction of space-time and renormalization in the AdS / CFT correspondence, Commun. Math. Phys. 217 (2001) 595–622, [hep-th/0002230].
- [40] J. Hammersley, Extracting the bulk metric from boundary information in asymptotically AdS spacetimes, JHEP 12 (2006) 047, [hep-th/0609202].
- [41] V. E. Hubeny, H. Liu and M. Rangamani, Bulk-cone singularities & signatures of horizon formation in AdS/CFT, JHEP 01 (2007) 009, [hep-th/0610041].
- [42] J. Hammersley, Numerical metric extraction in AdS/CFT, Gen. Rel. Grav. 40 (2008) 1619–1652, [0705.0159].
- [43] S. Bilson, Extracting spacetimes using the AdS/CFT conjecture, JHEP **08** (2008) 073, [0807.3695].
- [44] S. Bilson, Extracting Spacetimes using the AdS/CFT Conjecture: Part II, JHEP **02** (2011) 050, [1012.1812].
- [45] V. E. Hubeny, Extremal surfaces as bulk probes in AdS/CFT, JHEP 07 (2012) 093, [1203.1044].
- [46] N. Jokela, K. Rummukainen, A. Salami, A. Pönni and T. Rindlisbacher, Progress in the lattice evaluation of entanglement entropy of three-dimensional Yang-Mills theories and hologra JHEP 12 (2023) 137, [2304.08949].
- [47] V. Balasubramanian, B. D. Chowdhury, B. Czech, J. de Boer and M. P. Heller, Bulk curves from boundary data in holography, Phys. Rev. D 89 (2014) 086004, [1310.4204].
- [48] R. C. Myers, J. Rao and S. Sugishita, <u>Holographic Holes in Higher Dimensions</u>, <u>JHEP</u> **06** (2014) 044, [1403.3416].
- [49] B. Czech and L. Lamprou, <u>Holographic definition of points and distances</u>, <u>Phys. Rev. D</u> **90** (2014) 106005, [1409.4473].
- [50] N. Engelhardt and G. T. Horowitz, <u>Towards a Reconstruction of General Bulk Metrics</u>, <u>Class. Quant. Grav.</u> 34 (2017) 015004, [1605.01070].
- [51] N. Engelhardt and G. T. Horowitz, <u>Recovering the spacetime metric from a holographic dual</u>, <u>Adv. Theor. Math. Phys.</u> 21 (2017) 1635–1653, [1612.00391].

- [52] S. R. Roy and D. Sarkar, <u>Bulk metric reconstruction from boundary entanglement</u>, <u>Phys.</u> Rev. D **98** (2018) 066017, [1801.07280].
- [53] D. Kabat and G. Lifschytz, <u>Emergence of spacetime from the algebra of total modular Hamiltonians</u>, <u>JHEP</u> **05** (2019) 017, [1812.02915].
- [54] K. Hashimoto, Building bulk from Wilson loops, PTEP **2021** (2021) 023B04, [2008.10883].
- [55] S. Caron-Huot, <u>Holographic cameras: an eye for the bulk</u>, <u>JHEP</u> **03** (2023) 047, [2211.11791].
- [56] K. Hashimoto and R. Watanabe, Bulk reconstruction of metrics inside black holes by complexity, JHEP 09 (2021) 165, [2103.13186].
- [57] W.-B. Xu and S.-F. Wu, Reconstructing black hole exteriors and interiors using entanglement and complexity, JHEP 07 (2023) 083, [2305.01330].
- [58] J. M. Maldacena, <u>Eternal black holes in anti-de Sitter</u>, <u>JHEP</u> **04** (2003) 021, [hep-th/0106112].
- [59] M. Van Raamsdonk, <u>Building up spacetime with quantum entanglement</u>, <u>Gen. Rel. Grav.</u> 42 (2010) 2323–2329, [1005.3035].
- [60] B. Swingle, Entanglement Renormalization and Holography, Phys. Rev. D 86 (2012) 065007, [0905.1317].
- [61] J. Maldacena and L. Susskind, <u>Cool horizons for entangled black holes</u>, <u>Fortsch. Phys.</u> 61 (2013) 781–811, [1306.0533].
- [62] S. Ryu and T. Takayanagi, <u>Aspects of Holographic Entanglement Entropy</u>, <u>JHEP</u> 08 (2006) 045, [hep-th/0605073].
- [63] G. Vidal, Class of Quantum Many-Body States That Can Be Efficiently Simulated, Phys. Rev. Lett. **101** (2008) 110501, [quant-ph/0610099].
- [64] G. Vidal, Entanglement Renormalization, Phys. Rev. Lett. 99 (2007) 220405, [cond-mat/0512165].
- [65] A. Milsted and G. Vidal, Geometric interpretation of the multi-scale entanglement renormalization ansatz, 1812.00529.
- [66] K. Hashimoto, S. Sugishita, A. Tanaka and A. Tomiya, <u>Deep learning and the AdS/CFT correspondence</u>, <u>Phys. Rev. D</u> 98 (2018) 046019, [1802.08313].
- [67] K. Hashimoto, S. Sugishita, A. Tanaka and A. Tomiya, Deep Learning and Holographic QCD, Phys. Rev. D 98 (2018) 106014, [1809.10536].
- [68] K. Hashimoto, AdS/CFT correspondence as a deep Boltzmann machine, Phys. Rev. D 99 (2019) 106017, [1903.04951].
- [69] J. Tan and C.-B. Chen, <u>Deep learning the holographic black hole with charge</u>, <u>Int. J. Mod. Phys. D 28</u> (2019) 1950153, [1908.01470].
- [70] T. Akutagawa, K. Hashimoto and T. Sumimoto, <u>Deep Learning and AdS/QCD</u>, <u>Phys. Rev.</u> <u>D</u> 102 (2020) 026020, [2005.02636].

- [71] Y.-K. Yan, S.-F. Wu, X.-H. Ge and Y. Tian,
 <u>Deep learning black hole metrics from shear viscosity</u>, <u>Phys. Rev. D</u> **102** (4, 2020) 101902,
 [2004.12112].
- [72] K. Hashimoto, H.-Y. Hu and Y.-Z. You, Neural ordinary differential equation and holographic quantum chromodynamics, Mach. Learn. Sci. Tech. 2 (2021) 035011, [2006.00712].
- [73] K. Hashimoto, K. Ohashi and T. Sumimoto, Deriving the dilaton potential in improved holographic QCD from the meson spectrum, Phys. Rev. D 105 (2022) 106008, [2108.08091].
- [74] R. Katsube, W.-H. Tam, M. Hotta and Y. Nambu, <u>Deep learning metric detectors in general relativity</u>, <u>Phys. Rev. D</u> 106 (2022) 044051, [2206.03006].
- [75] K. Hashimoto, K. Ohashi and T. Sumimoto, Deriving the dilaton potential in improved holographic QCD from the chiral condensate, PTEP 2023 (2023) 033B01, [2209.04638].
- [76] K. Li, Y. Ling, P. Liu and M.-H. Wu, <u>Learning the black hole metric from holographic conductivity</u>, <u>Phys. Rev. D</u> 107 (2023) 066021, [2209.05203].
- [77] C. Park, C.-O. Hwang, K. Cho and S.-J. Kim, <u>Dual geometry of entanglement entropy via deep learning</u>, <u>Phys. Rev. D</u> **106** (2022) 106017, [2205.04445].
- [78] C. Park, S. Kim and J. H. Lee, Holography Transformer, 2311.01724.
- [79] K. Zhou, L. Wang, L.-G. Pang and S. Shi, <u>Exploring QCD matter in extreme conditions with Machine Learning</u>, <u>Prog. Part. Nucl. Phys. 135</u> (2024) 104084, [2303.15136].
- [80] B. Ahn, H.-S. Jeong, K.-Y. Kim and K. Yun, <u>Deep learning bulk spacetime from boundary optical conductivity</u>, <u>JHEP</u> **03** (2024) 141, [2401.00939].
- [81] Z.-F. Gu, Y.-K. Yan and S.-F. Wu, Neural ODEs for holographic transport models without translation symmetry, 2401.09946.
- [82] X. Chen and M. Huang,
 Machine learning holographic black hole from lattice QCD equation of state, Phys. Rev. D 109 (2024) L051902, [2401.06417].
- [83] K. Hashimoto, Y. Hirono and A. Sannai, Unification of Symmetries Inside Neural Networks: Transformer, Feedforward and Neural ODE, 2402.02362.
- [84] X. Chen and M. Huang, Flavor dependent Critical endpoint from holographic QCD through machine learning, 2405.06179.
- [85] Y. Bea, R. Jimenez, D. Mateos, S. Liu, P. Protopapas, P. Tarancón-Álvarez et al., Gravitational Duals from Equations of State, 2403.14763.
- [86] Y.-Z. You, Z. Yang and X.-L. Qi,

- Machine Learning Spatial Geometry from Entanglement Features, Phys. Rev. B **97** (2018) 045153, [1709.01223].
- [87] H.-Y. Hu, S.-H. Li, L. Wang and Y.-Z. You, Machine Learning Holographic Mapping by Neural Network Renormalization Group, Rev. Res. 2 (2020) 023369, [1903.00804].
- [88] X. Han and S. A. Hartnoll, <u>Deep Quantum Geometry of Matrices</u>, <u>Phys. Rev. X</u> 10 (2020) 011069, [1906.08781].
- [89] J. Lam and Y.-Z. You, Machine learning statistical gravity from multi-region entanglement entropy, Phys. Rev. Res. 3 (2021) 043199, [2110.01115].
- [90] M. Song, M. S. H. Oh, Y. Ahn and K.-Y. Kima, <u>AdS/Deep-Learning made easy: simple examples</u>, <u>Chin. Phys. C</u> 45 (2021) 073111, [2011.13726].
- [91] D. Areán, H.-S. Jeong, J. F. Pedraza and L.-C. Qu, <u>Black hole interiors and the kasner</u> universe: an analytic approach, to appear 2024.
- [92] S. S. Gubser and F. D. Rocha, <u>Peculiar properties of a charged dilatonic black hole in AdS₅, Phys.Rev.</u> D81 (2010) 046001, [0911.2898].
- [93] S. A. Hartnoll, C. P. Herzog and G. T. Horowitz, <u>Building a Holographic Superconductor</u>, Phys.Rev.Lett. **101** (2008) 031601, [0803.3295].
- [94] S. A. Hartnoll, C. P. Herzog and G. T. Horowitz, <u>Holographic Superconductors</u>, <u>JHEP</u> 0812 (2008) 015, [0810.1563].
- [95] M. Cvetic, M. J. Duff, P. Hoxha, J. T. Liu, H. Lu, J. X. Lu et al., Embedding AdS black holes in ten-dimensions and eleven-dimensions, Nucl. Phys. B 558 (1999) 96-126, [hep-th/9903214].
- [96] S. S. Gubser, C. P. Herzog, S. S. Pufu and T. Tesileanu, Superconductors from Superstrings, Phys. Rev. Lett. 103 (2009) 141601, [0907.3510].
- [97] J. P. Gauntlett, J. Sonner and T. Wiseman, <u>Holographic superconductivity in M-Theory</u>, <u>Phys.Rev.Lett.</u> **103** (2009) 151601, [0907.3796].
- [98] Q. Miao and T. Barthel, Eigenstate entanglement: Crossover from the ground state to volume laws, Phys. Rev. Lett. 127 (2021) 040603, [1905.07760].
- [99] A. Polyanin and A. Manzhirov, Handbook of Integral Equations. Taylor & Francis, 1998.
- [100] T. Andrade and B. Withers, <u>A simple holographic model of momentum relaxation</u>, <u>JHEP</u> 1405 (2014) 101, [1311.5157].
- [101] D. Vegh, Holography without translational symmetry, 1301.0537.
- [102] M. Baggioli, K.-Y. Kim, L. Li and W.-J. Li, Holographic Axion Model: a simple gravitational tool for quantum matter, Sci. China Phys. Mech. Astron. 64 (2021) 270001, [2101.01892].
- [103] J. Zaanen, Y.-W. Sun, Y. Liu and K. Schalm, Holographic Duality in Condensed Matter Physics. Cambridge Univ. Press, 2015.
- [104] S. A. Hartnoll, A. Lucas and S. Sachdev, Holographic quantum matter, 1612.07324.

- [105] M. Baggioli, <u>Applied Holography: A Practical Mini-Course</u>, other thesis, Madrid, IFT, 2019. 10.1007/978-3-030-35184-7.
- [106] M. Natsuume, AdS/CFT Duality User Guide, vol. 903. 2015, 10.1007/978-4-431-55441-7.
- [107] J. Zaanen, Lectures on quantum supreme matter, 2110.00961.
- [108] T. Faulkner, N. Iqbal, H. Liu, J. McGreevy and D. Vegh, From Black Holes to Strange Metals, 1003.1728.
- [109] R. A. Davison, K. Schalm and J. Zaanen, <u>Holographic duality and the resistivity of strange metals</u>, <u>Phys. Rev.</u> **B89** (2014) 245116, [1311.2451].
- [110] B. Goutéraux, Charge transport in holography with momentum dissipation, JHEP 1404 (2014) 181, [1401.5436].
- [111] E. Blauvelt, S. Cremonini, A. Hoover, L. Li and S. Waskie, <u>Holographic model for the anomalous scalings of the cuprates</u>, <u>Phys. Rev.</u> **D97** (2018) 061901, [1710.01326].
- [112] H.-S. Jeong, K.-Y. Kim and C. Niu, <u>Linear-T resistivity at high temperature</u>, <u>JHEP</u> 10 (2018) 191, [1806.07739].
- [113] L. Alberte, M. Ammon, A. Jiménez-Alba, M. Baggioli and O. Pujolàs, <u>Holographic</u> phonons, Phys. Rev. Lett. **120** (Apr. 2018) 171602.
- [114] M. Ammon, M. Baggioli and A. Jimenez-Alba, A Unified Description of Translational Symmetry Breaking in Holography, 1904.05785.
- [115] Y. Ahn, H.-S. Jeong, D. Ahn and K.-Y. Kim,

 <u>Linear-T resistivity from low to high temperature: axion-dilaton theories</u>, <u>JHEP</u> **04** (2020) 153, [1907.12168].
- [116] H.-S. Jeong and K.-Y. Kim, <u>Homes' law in holographic superconductor with linear-T resistivity</u>, <u>JHEP</u> **03** (2022) 060, [2112.01153].
- [117] M. Baggioli and B. Goutéraux,
 Colloquium: Hydrodynamics and holography of charge density wave phases, Rev. Mod. Phys. 95 (2023) 011001, [2203.03298].
- [118] F. Balm et al., T-linear resistivity, optical conductivity, and Planckian transport for a holographic local quantum critical meta Phys. Rev. B 108 (2023) 125145, [2211.05492].
- [119] Y. Ahn, M. Baggioli, H.-S. Jeong and K.-Y. Kim, Inability of linear axion holographic Gubser-Rocha model to capture all the transport anomalies of strange metables. Rev. B 108 (2023) 235104, [2307.04433].
- [120] R. A. Davison and B. Goutéraux, Momentum dissipation and effective theories of coherent and incoherent transport, 1411.1062.
- [121] M. Blake and A. Donos, <u>Diffusion and Chaos from near AdS₂ horizons</u>, <u>JHEP</u> **02** (2017) 013, [1611.09380].
- [122] A. Amoretti, M. Baggioli, N. Magnoli and D. Musso, Chasing the cuprates with dilatonic dyons, JHEP 06 (2016) 113, [1603.03029].

- [123] M. Blake, R. A. Davison and S. Sachdev, Thermal diffusivity and chaos in metals without quasiparticles, 1705.07896.
- [124] M. Baggioli and W.-J. Li, <u>Diffusivities bounds and chaos in holographic Horndeski theories</u>, JHEP 07 (2017) 055, [1705.01766].
- [125] H.-S. Jeong, Y. Ahn, D. Ahn, C. Niu, W.-J. Li and K.-Y. Kim, <u>Thermal diffusivity and butterfly velocity in anisotropic Q-Lattice models</u>, <u>JHEP</u> **01** (2018) 140, [1708.08822].
- [126] D. Giataganas, U. Gürsoy and J. F. Pedraza, <u>Strongly-coupled anisotropic gauge theories and holography</u>, <u>Phys. Rev. Lett.</u> 121 (2018) 121601, [1708.05691].
- [127] R. A. Davison, S. A. Gentle and B. Goutéraux,

 Slow relaxation and diffusion in holographic quantum critical phases, Phys. Rev. Lett. 123

 (2019) 141601, [1808.05659].
- [128] M. Blake, R. A. Davison, S. Grozdanov and H. Liu, Many-body chaos and energy dynamics in holography, JHEP 10 (2018) 035, [1809.01169].
- [129] H.-S. Jeong, K.-Y. Kim, Y. Seo, S.-J. Sin and S.-Y. Wu, <u>Holographic Spectral Functions with Momentum Relaxation</u>, <u>Phys. Rev. D</u> 102 (2020) 026017, [1910.11034].
- [130] D. Arean, R. A. Davison, B. Goutéraux and K. Suzuki, <u>Hydrodynamic Diffusion and Its Breakdown near AdS2 Quantum Critical Points</u>, <u>Phys.</u> <u>Rev. X 11 (2021) 031024</u>, [2011.12301].
- [131] Y. Liu and X.-M. Wu, <u>Breakdown of hydrodynamics from holographic pole collision</u>, <u>JHEP</u> **01** (2022) 155, [2111.07770].
- [132] H.-S. Jeong, K.-Y. Kim and Y.-W. Sun, Bound of diffusion constants from pole-skipping points: spontaneous symmetry breaking and magnetic field, JHEP 07 (2021) 105, [2104.13084].
- [133] N. Wu, M. Baggioli and W.-J. Li,

 On the universality of AdS₂ diffusion bounds and the breakdown of linearized hydrodynamics,

 JHEP **05** (2021) 014, [2102.05810].
- [134] H.-S. Jeong, K.-Y. Kim and Y.-W. Sun, The breakdown of magneto-hydrodynamics near AdS₂ fixed point and energy diffusion bound, JHEP 02 (2022) 006, [2105.03882].
- [135] K.-B. Huh, H.-S. Jeong, K.-Y. Kim and Y.-W. Sun, Upper bound of the charge diffusion constant in holography, JHEP 07 (2022) 013, [2111.07515].
- [136] H.-S. Jeong, K.-Y. Kim and Y.-W. Sun, Quasi-normal modes of dyonic black holes and magneto-hydrodynamics, JHEP 07 (2022) 065, [2203.02642].
- [137] M. Baggioli, S. Grieninger, S. Grozdanov and Z. Lu, Aspects of univalence in holographic axion models, JHEP 11 (2022) 032, [2205.06076].
- [138] H.-S. Jeong, Quantum chaos and pole-skipping in a semilocally critical IR fixed point, 2309.13412.

- [139] Y. Ahn, V. Jahnke, H.-S. Jeong, C.-W. Ji, K.-Y. Kim and M. Nishida, On pole-skipping with gauge-invariant variables in holographic axion theories, 2402.12951.
- [140] Z. Zhao, W. Cai and S. Ishigaki, Doped holographic superconductors in the Gubser–Rocha model, Commun. Theor. Phys. 76 (2024) 045201, [2309.14851].
- [141] M. Baggioli and O. Pujolas, Holographic Polarons, the Metal-Insulator Transition and Massive Gravity, 1411.1003.
- [142] L. Alberte, M. Baggioli, A. Khmelnitsky and O. Pujolas, Solid Holography and Massive Gravity, JHEP 02 (2016) 114, [1510.09089].
- [143] A. Amoretti, D. Areán, R. Argurio, D. Musso and L. A. Pando Zayas, <u>A holographic perspective on phonons and pseudo-phonons</u>, <u>JHEP</u> 05 (2017) 051, [1611.09344].
- [144] L. Alberte, M. Ammon, A. Jiménez-Alba, M. Baggioli and O. Pujolàs, Holographic Phonons, Phys. Rev. Lett. 120 (2018) 171602, [1711.03100].
- [145] A. Amoretti, D. Areán, B. Goutéraux and D. Musso, <u>Effective holographic theory of charge density waves</u>, <u>Phys. Rev.</u> **D97** (2018) 086017, [1711.06610].
- [146] A. Amoretti, D. Aren, B. Goutraux and D. Musso, DC resistivity of quantum critical, charge density wave states from gauge-gravity duality, Phys. Rev. Lett. 120 (2018) 171603, [1712.07994].
- [147] L. Alberte, M. Ammon, M. Baggioli, A. Jimnez and O. Pujol s, Black hole elasticity and gapped transverse phonons in holography, JHEP 01 (2018) 129, [1708.08477].
- [148] T. Andrade, M. Baggioli, A. Krikun and N. Poovuttikul, Pinning of longitudinal phonons in holographic spontaneous helices, JHEP 02 (2018) 085, [1708.08306].
- [149] A. Amoretti, D. Aren, B. Goutraux and D. Musso, A holographic strange metal with slowly fluctuating translational order, 1812.08118.
- [150] A. Amoretti, D. Areán, B. Goutéraux and D. Musso, <u>Diffusion and universal relaxation of holographic phonons</u>, <u>JHEP</u> 10 (2019) 068, [1904.11445].
- [151] M. Baggioli and S. Grieninger, Zoology of solid \& fluid holography — Goldstone modes and phase relaxation, JHEP 10 (2019) 235, [1905.09488].
- [152] A. Amoretti, D. Areán, B. Goutéraux and D. Musso, Gapless and gapped holographic phonons, JHEP 01 (2020) 058, [1910.11330].
- [153] M. Ammon, M. Baggioli, S. Gray and S. Grieninger, Longitudinal Sound and Diffusion in Holographic Massive Gravity, JHEP 10 (2019) 064, [1905.09164].
- [154] M. Baggioli, S. Grieninger and L. Li, Magnetophonons & type-B Goldstones from Hydrodynamics to Holography, 2005.01725.

- [155] A. Amoretti, D. Arean, D. K. Brattan and N. Magnoli, <u>Hydrodynamic magneto-transport in charge density wave states</u>, <u>JHEP</u> **05** (2021) 027, [2101.05343].
- [156] A. Amoretti, D. Arean, D. K. Brattan and L. Martinoia, <u>Hydrodynamic magneto-transport in holographic charge density wave states</u>, <u>JHEP</u> 11 (2021) 011, [2107.00519].
- [157] X.-J. Wang and W.-J. Li, <u>Holographic phonons by gauge-axion coupling</u>, <u>JHEP</u> **07** (2021) 131, [2105.07225].
- [158] Y.-Y. Zhong and W.-J. Li, Transverse Goldstone mode in holographic fluids with broken translations, <u>Eur. Phys. J. C</u> 82 (2022) 511, [2202.05437].
- [159] M. Bajec, S. Grozdanov and A. Soloviev, Spectra of correlators in the relaxation time approximation of kinetic theory, 2403.17769.
- [160] M. Reza Mohammadi Mozaffar, A. Mollabashi and F. Omidi, Non-local Probes in Holographic Theories with Momentum Relaxation, JHEP 10 (2016) 135, [1608.08781].
- [161] D. M. Yekta, H. Babaei-Aghbolagh, K. Babaei Velni and H. Mohammadzadeh, Holographic complexity for black branes with momentum relaxation, Phys. Rev. D 104 (2021) 086025, [2009.01340].
- [162] Y.-Z. Li and X.-M. Kuang, Probes of holographic thermalization in a simple model with momentum relaxation, Nucl. Phys. B 956 (2020) 115043, [1911.11980].
- [163] Y.-T. Zhou, X.-M. Kuang, Y.-Z. Li and J.-P. Wu, Holographic subregion complexity under a thermal quench in an Einstein-Maxwell-axion theory with momentu Phys. Rev. D 101 (2020) 106024, [1912.03479].
- [164] Y.-f. Huang, Z.-j. Shi, C. Niu, C.-y. Zhang and P. Liu, Mixed State Entanglement for Holographic Axion Model, <u>Eur. Phys. J. C</u> 80 (2020) 426, [1911.10977].
- [165] S. A. Hosseini Mansoori, O. Luongo, S. Mancini, M. Mirjalali, M. Rafiee and A. Tavanfar, Planar black holes in holographic axion gravity: Islands, Page times, and scrambling times, Phys. Rev. D 106 (2022) 126018, [2209.00253].
- [166] W. E, A proposal on machine learning via dynamical systems, Communications in Mathematics and Statistics 5 (02, 2017) 1–11.
- [167] K. He, X. Zhang, S. Ren and J. Sun, <u>Deep residual learning for image recognition</u>, in <u>2016</u> <u>IEEE Conference on Computer Vision and Pattern Recognition (CVPR)</u>, pp. 770–778, 2016. <u>DOI</u>.
- [168] R. T. Q. Chen, Y. Rubanova, J. Bettencourt and D. Duvenaud, <u>Neural ordinary differential</u> equations, 1806.07366.
- [169] A. Paszke, S. Gross, F. Massa, A. Lerer, J. Bradbury, G. Chanan et al., <u>Pytorch: An imperative style, high-performance deep learning library</u>, in <u>Advances in Neural Information Processing Systems 32</u>, pp. 8024–8035. Curran Associates, Inc., 2019.
- [170] P. Gómez, H. H. Toftevaag and G. Meoni,

- torchquad: Numerical Integration in Arbitrary Dimensions with PyTorch, J. Open Source Softw. 6 (2021) 3439.
- [171] R. J. Anantua, S. A. Hartnoll, V. L. Martin and D. M. Ramirez, The Pauli exclusion principle at strong coupling: Holographic matter and momentum space, JHEP 1303 (2013) 104, [1210.1590].
- [172] X.-H. Ge and Z. Xu, <u>Thermo-electric transport of dyonic Gubser-Rocha black holes</u>, <u>JHEP</u> 03 (2024) 069, [2310.12067].
- [173] Z. Wang, X.-H. Ge and S. Ishigaki, Dependence of the critical temperature and disorder in holographic superconductors on superfluid density, 2312.16029.
- [174] C. P. Herzog, <u>Lectures on Holographic Superfluidity and Superconductivity</u>, <u>J.Phys.A</u> A42 (2009) 343001, [0904.1975].
- [175] R.-G. Cai, L. Li, L.-F. Li and R.-Q. Yang, Introduction to Holographic Superconductor Models, Sci. China Phys. Mech. Astron. 58 (2015) 060401, [1502.00437].
- [176] I. Amado, M. Kaminski and K. Landsteiner, Hydrodynamics of Holographic Superconductors, JHEP 0905 (2009) 021, [0903.2209].
- [177] D. Arean, M. Baggioli, S. Grieninger and K. Landsteiner, A holographic superfluid symphony, JHEP 11 (2021) 206, [2107.08802].
- [178] H.-S. Jeong, M. Baggioli, K.-Y. Kim and Y.-W. Sun, Collective dynamics and the Anderson-Higgs mechanism in a bona fide holographic superconductor, JHEP 03 (2023) 206, [2302.02364].
- [179] N. Jokela and A. Pönni, <u>Towards precision holography</u>, <u>Phys. Rev. D</u> **103** (2021) 026010, [2007.00010].
- [180] Q. Miao and T. Barthel, Eigenstate entanglement scaling for critical interacting spin chains, Quantum 6 (2022) 642, [2010.07265].
- [181] R. Shankar, Renormalization-group approach to interacting fermions, Reviews of Modern Physics 66 (1994) 129–192.
- [182] S. Sachdev, Quantum Phase Transitions. Cambridge University Press, 2 ed., 2011.
- [183] T. Senthil, <u>Critical fermi surfaces and non-fermi liquid metals</u>, <u>Physical Review B</u> **78** (2008)
- [184] H. Liu and M. Mezei, <u>Probing renormalization group flows using entanglement entropy</u>, JHEP **01** (2014) 098, [1309.6935].
- [185] N. W. Ashcroft and N. D. Mermin, Solid State Physics. Holt-Saunders, 1976.
- [186] C. Kittel, Introduction to Solid State Physics. Wiley, 8 ed., 2004.
- [187] L. Susskind, Entanglement is not enough, Fortsch. Phys. 64 (2016) 49–71, [1411.0690].
- [188] L. Susskind, Computational Complexity and Black Hole Horizons, Fortsch. Phys. **64** (2016) 24–43, [1403.5695].
- [189] J. Couch, W. Fischler and P. H. Nguyen, Noether charge, black hole volume, and complexity, JHEP 03 (2017) 119, [1610.02038].

- [190] A. Belin, R. C. Myers, S.-M. Ruan, G. Sárosi and A. J. Speranza, Does Complexity Equal Anything?, Phys. Rev. Lett. 128 (2022) 081602, [2111.02429].
- [191] A. Frenkel, S. A. Hartnoll, J. Kruthoff and Z. D. Shi, Holographic flows from CFT to the Kasner universe, JHEP 08 (2020) 003, [2004.01192].